

SOIL MOISTURE MODELING AND SCALING USING PASSIVE  
MICROWAVE REMOTE SENSING

A Thesis

by

NARENDRA N. DAS

Submitted to the Office of Graduate Studies of  
Texas A&M University  
in partial fulfillment of the requirements for the degree of

MASTER OF SCIENCE

December 2005

Major Subject: Biological and Agricultural Engineering

SOIL MOISTURE MODELING AND SCALING USING PASSIVE  
MICROWAVE REMOTE SENSING

A Thesis

by

NARENDRA N. DAS

Submitted to the Office of Graduate Studies of  
Texas A&M University  
in partial fulfillment of the requirements for the degree of

MASTER OF SCIENCE

Approved by:

Chair of Committee,  
Committee Members,

Head of Department,

Binayak P. Mohanty  
Raghavan Srinivasan  
Clyde Munster  
Sorin Popescu  
Gerald Riskowski

December 2005

Major Subject: Biological and Agricultural Engineering

## ABSTRACT

Soil Moisture Modeling and Scaling Using Passive Microwave Remote Sensing.

(December 2005)

Narendra N. Das, B.E., Government Engineering College Raipur.

Chair of Advisory Committee: Dr. Binayak P. Mohanty

Soil moisture in the shallow subsurface is a primary hydrologic state governing land-atmosphere interaction at various scales. The primary objectives of this study are to model soil moisture in the root zone in a distributed manner and determine scaling properties of surface soil moisture using passive microwave remote sensing. The study was divided into two parts. For the first study, a root zone soil moisture assessment tool (SMAT) was developed in the ArcGIS platform by fully integrating a one-dimensional vadose zone hydrology model (HYDRUS-ET) with an ensemble Kalman filter (EnKF) data assimilation capability. The tool was tested with dataset from the Southern Great Plain 1997 (SGP97) hydrology remote sensing experiment. Results demonstrated that SMAT displayed a reasonable capability to generate soil moisture distribution at the desired resolution at various depths of the root zone in Little Washita watershed during the SGP97 hydrology remote sensing experiment. To improve the model performance, several outstanding issues need to be addressed in the future by: including 'effective' hydraulic parameters across spatial scales; implementing subsurface soil properties data bases using direct and indirect methods; incorporating appropriate hydrologic processes

across spatial scales; accounting uncertainties in forcing data; and preserving interactions for spatially correlated pixels.

The second study focused on spatial scaling properties of the Polarimetric Scanning Radiometer (PSR)-based remotely sensed surface soil moisture fields in a region with high row crop agriculture. A wavelet based multi-resolution technique was used to decompose the soil moisture fields into larger-scale average soil moisture fields and fluctuations in horizontal, diagonal and vertical directions at various resolutions. The specific objective was to relate soil moisture variability at the scale of the PSR footprint (800 m X 800 m) to larger scale average soil moisture field variability. We also investigated the scaling characteristics of fluctuation fields among various resolutions. The spatial structure of soil moisture exhibited linearity in the log-log dependency of the variance versus scale-factor, up to a scale factor of -2.6 (6100 m X 6100 m) irrespective of wet and dry conditions, whereas dry fields reflect nonlinear (multi-scaling) behavior at larger scale-factors.

To my dear parents, loving wife, and daughter.

## ACKNOWLEDGEMENTS

First of all, I would like to thank my parents, whose love and support brought me to this juncture of my life. Special thanks go to my wife for her constant support and contribution in my every endeavor. I would like to take this opportunity to extend my thanks to my late father-in-law, my sisters, and all my friends for their motivation and support.

Gratitude also goes to my academic advisor and mentor, Dr. Binayak Mohanty, who offered tremendous help and support. As my guide he offered ideas and timely suggestions for my research work. In addition to continued funding, Dr. Binayak Mohanty always gave me ample space and liberty to conduct my research. I would also like to thank Dr. Raghavan Srinivasan, Dr. Clyde Munster, and Dr. Sorin Popescu for their guidance and support during my research work. Moreover, I am indebted to Dr. Fuqing Zhang and Sara Friedman for introducing me to the concept of data assimilation and ensemble Kalman filter. Very special thanks go to my brother-in-law, Saurajit Kanungo, and his wife, Savita Kanungo, who provided encouragement and support to my family during my field experiments. Surajit, Raghu, and Deb very often provided helpful advice and freely shared their time with me.

I would also like to thank Dr. Gary Heathman and Dr. Rajat Bindlish for sharing experiment dataset for my research work. I wish to thank NSIDC, USDA and NOAA for the valuable data. I also acknowledge the support of NASA fellowship (ESSF/03-000-0191), NASA grants (NAG5-11702).

Last, but definitely not the least, I would like to extend my special thanks and love to my daughter for her love and support.

## TABLE OF CONTENTS

	Page
ABSTRACT .....	iii
DEDICATION .....	iv
ACKNOWLEDGEMENTS .....	vi
TABLE OF CONTENTS .....	viii
LIST OF TABLES .....	ix
LIST OF FIGURES.....	x
CHAPTER	
I    GENERAL INTRODUCTION.....	1
II   ROOT ZONE SOIL MOISTURE ASSESSMENT USING REMOTE SENSING AND VADOSE ZONE MODELING.....	5
Introduction .....	6
Materials and Methods .....	12
Results and Discussion.....	28
Conclusion.....	43
III  SCALING OF SURFACE SOIL MOISTURE FIELDS DURING SMEX02.....	45
Introduction .....	46
Materials and Methods .....	50
Results and Discussion.....	60
Conclusion.....	72
IV   GENERAL CONCLUSIONS .....	74
REFERENCES.....	76
VITA .....	85



## LIST OF TABLES

TABLE	Page
II-1: Average hydraulic properties for different soil textures (Carsel and Parrish, 1988). .....	17
II-2. Definition, values, and sources for the parameters used in HYDRUS-ET. ....	21
II-3. Comparison of field soil moisture measurements and model results from Day of Year (DOY) 170 to 197 at 02-NOAA, Micronet-133, and Micronet-149. ....	30
III-1. Results of regression: slope $s(p)$ , coefficient of determination $R^2$ for order of moment versus scale-factors in horizontal, vertical and diagonal directions stationary fluctuation components) for PSR based soil moisture estimates of SMEX02.....	68

## LIST OF FIGURES

FIGURE	Page
II-1. Little Washita (LW) watershed with Micronet and NOAA sites used in the study. ....	13
II-2. Little Washita (LW) watershed soil map resampled at a resolution of 800 X 800 m. (SL: sandy loam, SiL: silty loam, L: loam, Cl: clay, CL: clay loam, S: sand, SiCL: silty clay loam). ....	15
II-3. Landuse landcover (LULC) for Little Washita (LW) watershed resampled at a resolution of 800 X 800 m. ....	16
II-4. Schematic representation of the Soil Moisture Assessment Tool (SMAT). ....	18
II-5. Site Micronet-133 temporal series of soil moisture at a) surface, b) 0-0.15 m, c) 0.15-0.30 m, and d) 0.45-0.60 m. (DOY: day of year, EnKF: ensemble Kalman filter, Meas: Measured). ....	31
II-6. Site Micronet-149 temporal series of soil moisture at a) surface, b) 0-0.15 m, c) 0.15-0.30 m, and d) 0.45-0.60 m. (DOY: day of year, EnKF: ensemble Kalman filter, Meas: Measured). ....	35
II-7. Site 02-NOAA temporal series of soil moisture at a) surface, b) 0-0.15 m, c) 0.15-0.30 m, and d) 0.45-0.60 m. (DOY: day of year, EnKF: ensemble Kalman filter, Meas: Measured). ....	38
II-8. Model predicted soil moisture grids at different depths across Little Washita (LW) watershed Day of Year (DOY)193 (12th July 1997) at the depth of (a) 0.05 m, (b) 0.2 m, (c) 0.4 m and (d) 0.6 m. ....	42
III-1. Location of SMEX02 experiment and IOWA regional study area (Bindlish et al. 2005). ....	51

FIGURE	Page
III-2. PSR (C-band single channel) based soil moisture estimates over the regional area during SMEX02.....	52
III-3. Haar wavelet decomposition of a PSR based soil moisture field. (a) Representation of original soil moisture field on June 25th 2005 of resolution 800 m X 800 m. (b) Average field A1 (top left quadrant) and three fluctuation fields D1h (horizontal component: top right quadrant), D1d (diagonal component: bottom right quadrant), and D1v (vertical component: bottom left quadrant) of resolution 1600 m X 1600 m.....	58
III-4. Mean of soil moisture against log of scale-factors. ....	61
III-5. Dependencies of the variance of soil moisture against scale – factors in a log-log plot. ....	62
III-6. (a) Linear fit for moment of order four versus scale-factors on a log-log plot for average soil moisture fields of June 29th (slope $s(p) = -0.54$ , and $R^2 = 0.85$ ) and July 11th 2002 (slope $s(p) = -0.17$ , and $R^2 = 0.9$ ). (b) Deviation and conformance to simple scaling in the change of slopes with respect to order of moments for soil moisture fields of June 29th and July 11th 2002 (SMEX02), respectively.....	65
III-7. Wavelet variance versus scale factor in log-log plot for fluctuation fields (horizontal direction) on June 29th and July 11th 2002 (SMEX02). ....	66
III-8. Slope $s(p)$ versus order of moment $p$ plots for fluctuations fields on June 29th 2005 (SMEX02): (a) horizontal, (b) diagonal and (c) vertical directions.....	69
III-9. Slope $s(p)$ versus order of moment $p$ plots for fluctuations fields on July 11th 2005 (SMEX02): (a) horizontal, (b) diagonal and (c) vertical directions.....	70

## CHAPTER I

### GENERAL INTRODUCTION

A very small proportion (0.15%) of fresh water on Earth is present as soil moisture (Dingman 1994). This small proportion of water (soil moisture) has an important influence in hydrology and meteorology. At the land-atmosphere boundary, soil moisture modulates the land-atmosphere interaction by partitioning rainfall into infiltration and runoff, and solar radiation into latent heat flux and sensible heat flux. Soil moisture also impacts the plant growth which affects ecological patterns and agricultural production. The hydrological, meteorological and ecological processes are influenced by spatio-temporal variability of soil moisture at the soil surface and in the root zone that in turn is affected by soil properties (Famiglietti et al., 1999), precipitation distribution (Jackson 1993), topographic features (Wilson and Gallant, 2000), and vegetation characteristics (Hupet and Vanclooster, 2002).

The heterogeneity present in the soil is due to difference in texture, porosity, structure and organic matters contents, which affects the soil hydraulic properties. The soil hydraulic properties mostly control the vertical and lateral transmission of soil moisture through the soil. Hawley et al. (1982) found significant variability in surface

---

This thesis follows the style of *Vadose Zone Journal*.

soil moisture due to difference in soil texture and antecedent soil moisture. Soil moisture distribution is also affected by variability present in the precipitation patterns. Sellers et al. (1995) presented spatial heterogeneity introduced by rainfall and removed through dry-down dynamics. Variations in topography (slope, curvature and aspect) effect the distribution of soil moisture near the land surface. Slope angle have significant affects on infiltration, lateral drainage and runoff. Aspect influences solar irradiance and thus evapotranspiration and soil moisture. Curvature present in the landscape influences the convergence of the lateral flow. Studies have also found that soil moisture content is inversely proportional to relative elevation (Hawley et al. 1982; Nyberg 1996). Francis et al. (1986) found considerable difference in soil moisture content due to difference in vegetative cover. Vegetation influences soil moisture distribution by interfering in soil hydraulic properties through root activities, adding organic matters, interception, and evapotranspiration.

Soil moisture pattern (distribution) evolves from many different geophysical processes acting over different scales (Dubayah et al., 1997). The spatio-temporal variability of soil moisture influences hydrological and meteorological processes in a nonlinear manner. This nonlinearity introduces spatio-temporal scaling effects for soil moisture. Rodriguez-Iturbe et al. (1995) concluded that the variance of soil moisture follow a power law decay, typical of scaling processes, as a function of area over which soil moisture is observed.

The spatio-temporal variability of soil moisture imposes many challenges to measure and model the surface and the root zone soil moisture. Typically soil moisture is

measured *in-situ* or by remote sensing techniques. In-situ soil moisture measurement techniques can be used to continuously monitor soil moisture at various depths at a location but limited by its small support volume (few  $\text{cm}^3$ ). In-situ measurement techniques serve well for field plots or local-scale monitoring but are not very suitable for watershed or regional scale soil moisture observations. Remote sensing of soil moisture from air-/space-borne platforms has the ability to overcome this problem and provide large spatial coverage and temporal continuity. In the last three decades studies have successfully established the use of passive microwave remote sensing to measure the surface wetness (Engman and Gurney, 1991; Jackson, 1993; Njoku and Entekhabi, 1995; Jackson et al., 1999). The existing and proposed air-/space-borne passive microwave remote sensors typically provide regional or global scale soil moisture distributions at spatial resolutions ranging from several hundred square meters to several thousand square kilometers.

Typically, soil moisture state and energy/mass fluxes are simulated in Soil Vegetation Atmosphere Transfer (SVAT) scheme of any General Circulation Model (GCM) using surface soil moisture data from passive microwave remote sensing. The accuracy of SVAT models is usually restricted by unreliable estimates of root zone soil moisture (Koster and Milly, 1997) and its spatio-temporal scaling behavior. Despite the significance of root zone soil moisture in hydrological and meteorological predictions, research related to spatio-temporal modeling of root zone soil moisture and its scaling behavior at the regional/global scale is limited, hence this study.

The objective of this study is to model spatio-temporal distribution of root zone soil moisture and determine scaling properties of surface soil moisture using passive microwave remote sensing. The study is divided into two parts. First, a distributed root zone soil moisture assessment tool (SMAT) is developed in ArcGIS platform by fully integrating a one-dimensional vadose zone hydrology model (HYDRUS-ET) with ensemble Kalman filter (EnKF) data assimilation capability. Second part of this study focused on spatial scaling properties of Polarimetric Scanning Radiometer (PSR)-based remotely sensed soil moisture fields in a region with high row crop agriculture. Wavelet based multiresolution techniques was used to decompose the soil moisture fields into large-scale average soil moisture fields and fluctuations in horizontal, diagonal and vertical directions at various spatial resolutions.

## CHAPTER II

### ROOT ZONE SOIL MOISTURE ASSESSMENT USING REMOTE SENSING AND VADOSE ZONE MODELING

Soil moisture is an important hydrologic state variable critical to successful of many hydroclimatic and environmental predictions. Soil moisture varies both in space and time because of spatio-temporal variations in precipitation, soil properties, topographic features, and vegetation characteristics. In recent years, air- and space-borne remote sensing campaigns have successfully demonstrated the use of passive microwave remote sensing to map soil moisture status near the soil surface (0~0.05 m below the ground) at various spatial scales. In this study root zone (e.g., 0~0.6 m below the ground) soil moisture distributions were estimated across the Little Washita watershed (Oklahoma) by assimilating near-surface soil moisture data from remote sensing measurements using ESTAR (Electronically Scanned Thinned Array Radiometer) with an EnKF (Ensemble Kalman Filter) technique coupled with a numerical one-dimensional vadose zone flow model (HYDRUS-ET). The resulting distributed root zone soil moisture assessment tool (SMAT) is based on the concept of having parallel non-interacting streamtubes (hydrologic units) within a geographic information system (GIS) platform. The simulated soil moisture distribution at various depths and locations within the watershed were compared with measured profile soil moisture data using TDR (Time Domain Reflectometry). A reasonable agreement was found under favorable conditions between footprint-scale model estimations and point-scale field soil moisture



measurements in the root zone. However, uncertainties introduced by precipitation and soil hydraulic properties caused suboptimal performance of the integrated model. The SMAT holds great promise and flexibility to incorporate various data assimilation techniques, scaling, and other hydrological complexities across large landscapes. The integrated model can be useful for simulating profile soil moisture estimation, and for predicting transient soil moisture behavior for a range of hydrological and environmental applications.

### **Introduction**

Spatio-temporal distributions of soil moisture status in the root zone across large land areas provide important input for many agricultural, hydrological, and meteorological applications (Hanson et al., 1999). Also, estimation of root zone soil moisture at various temporal and spatial scales is key to strategic management of water resources. Root zone soil moisture is a critical storage parameter, which controls partitioning of energy and mass related to evapotranspiration and runoff (Georgakakos, 1996). Precipitation, soil texture, topography, land use, and a variety of meteorological variables influence the spatial distribution and temporal evolution of root zone soil moisture. Many studies at the SGP97 (Southern Great Plains 1997 hydrology experiment) site have examined how these variables influence the spatio-temporal distribution of soil moisture and surface fluxes (Famiglietti et al., 1999; Mohr et al., 2000; Mohanty et al., 2000a, 2000b; Mohanty and Skaggs, 2001; Bindlish et al., 2001;

Kustas et al., 2001; Wickel et al., 2001). The estimation of soil moisture and energy/mass exchange is simulated using Soil Vegetation Atmosphere Transfer models (SVAT). The accuracy of SVAT models is usually restricted by unreliable estimates of root zone soil moisture (Koster and Milly, 1997). Despite the significance of root zone soil moisture in hydrological and meteorological predictions, detailed spatio-temporal modeling of root zone soil moisture at the regional/global scale is often lacking.

Root zone soil moisture distributions are best assessed by periodic gravimetric sampling or by calibrated TDR techniques. At a particular location, soil moisture can be continuously monitored by calibrating segmented TDR probes (e.g., Hook and Livingston, 1996) or by multi-sensor capacitance probes (e.g., Starr and Paltineanu, 1998). Camillo and Schmutge (1983) retrieved root zone soil moisture estimates from surface measurement for dry soil with fully grown roots using a linear relationship between moisture content in the two soil layers based on a simple solution of Richards' equation. These techniques serve well for field plot or local-scale monitoring but are not feasible for watershed or regional scale. Remote sensing of soil moisture from air-/space-borne platforms has the ability to overcome this problem and provide large spatial coverage and temporal continuity. In the last three decades studies have successfully established the use of passive microwave remote sensing to measure the surface wetness (Engman and Gurney, 1991; Jackson, 1993; Njoku and Entekhabi, 1995; Jackson et al., 1999). These measurements described soil moisture in a thin soil layer, usually up to a depth of 0.05 m below the soil surface (Schmutge et al., 1974, 1977, 1980; Jackson and Schmutge, 1989). However, an associated problem, which hindered the measurement of

soil moisture from air/space using passive microwave techniques, is its coarse spatial and temporal resolution which is not consistent with the scale of hydrologic processes of interest.

Prevot et al. (1984) demonstrated that the soil water balance could be determined with equal accuracy using remotely sensed surface soil moisture estimates substituted for in situ observations. Smith and Newton (1983) developed a soil water simulation model that utilized remotely sensed data to predict profile soil moisture. In the recent past, studies have been conducted on improving assessment of profile soil moisture with the help of surface soil moisture observations (Kostov and Jackson, 1993; Entekhabi et al., 1994). Jackson (1993) elaborated four strategies using surface soil moisture data to estimate profile soil moisture: (i) statistical extrapolation of the surface observation, (ii) integration of surface observations in a profile water budget model, (iii) inversion of radiative transfer model, and (iv) the parametric profile model method. Kostov and Jackson, (1993) presented a detailed review of these basic approaches for estimating profile soil moisture using remotely sensed surface moisture data and concluded that the most promising approach to the problem of profile soil moisture estimation was the integration of remote sensing and computational modeling. An illustration of this concept has been provided by Entekhabi et al. (1994) in their theoretical approach for solving the inverse problem for soil moisture using sequential assimilation of remotely sensed surface data. Houser et al. (1998) studied the use of four-dimensional data assimilation methods in a macro-scale land hydrology model to generate root zone moisture fields on regular space and time intervals. Several other studies were conducted

using data from the Southern Great Plains 1997 (SGP97) hydrology experiment (Jackson et al., 1999), and tested these concepts at the point scale (Crosson et al., 2002; Starks et al., 2003; Heathman et al., 2003; Crow and Wood, 2003). Walker et al. (2001) explored the effects of observation depth and update interval on soil moisture profile retrieval and made a comparison of two commonly used assimilation techniques (i.e., direct insertion and Kalman filter) using synthetic data. They concluded that Kalman filter assimilation scheme is superior to the direct insertion assimilation scheme, and profile retrieval was unsuccessful for direct insertion using the surface node alone, with observations over some non-zero depth being required. The superiority of the Kalman filter lies in its ability to adjust the entire profile, while direct insertion can only alter the profile within the observation depth. On the contrary, Heathman et al. (2003) investigated profile soil water content using direct data assimilation in Root Zone Water Quality model at four field sites in the Little Washita (LW) River Experimental Watershed during SGP97, and found that direct insertion assimilation improved model estimates down to a depth of 0.30 m at all the sites considered in their study, and no significant improvement in soil water estimates below the 0.30 m depth. Crosson et al. (2002) applied the Kalman Filter based method for assimilating remotely sensed (ESTAR-based, during SGP97) soil moisture estimates in a point-scale testing scheme and found that even in the presence of highly inaccurate rainfall the model results in good agreement with observed soil moisture. Crow and Wood (2003) extended Ensemble Kalman Filter (EnKF) methodology to assimilate remotely sensed (ESTAR, SGP97) soil moisture data into a land surface model and validated against independent observations. They found that

root-zone soil moisture predictions made with the EnKF are more accurate than predictions derived from direct assimilation of ESTAR surface soil moisture imagery. Recently, Dunne and Entekhabi (2005) used ESTAR pixel and field data of SGP97 to investigate an ensemble-based reanalysis (ensemble based smoother) approach to land data assimilation. They demonstrated that smoothing improved the estimated soil moisture at the soil surface and at deeper depths over EnKF estimation. The performance of EnKF was also studied by Reichle et al. (2002) and Margulis et al. (2002), where soil moisture estimation is assessed by assimilating L-band (1.4 GHz) microwave observations into a land surface model. They showed that EnKF is a flexible and robust data assimilation technique that gives satisfactory estimates even for moderate ensemble size. From these, it is clear that EnKF offers several advantages over traditional methods of data assimilation for retrieving soil moisture from microwave remote sensing.

Generally, data assimilation is used in conjunction with a SVAT (land surface model, LSM) model. The model can be treated as a stand-alone program, which communicates with the filter through its input and output files. The filter provides a set of random initial conditions, parameters, and forcing variables to the land surface model. In turn, the model derives a time-dependent state vector that is passed to the filtering algorithm. This modularity makes it possible to use nearly any land surface model in a data assimilation procedure based on an EnKF. The most frequently used SVAT model with data assimilation are NOAH model (Chen et al., 1996), Variable Infiltration Capacity (VIC) model (Liang et al., 1996), Mosaic model (Koster and Suarez, 1996), and Common Land Model (CLM; Dai et al., 2003). The SVAT models typically include

a thin surface soil layer and one or more thicker layers as root zone and estimate soil moisture of each soil layer at the land-atmosphere boundary and the interfaces between the soil layers. The SVAT models run typically in an uncoupled fashion using a number of generic tools to manage the input and output data. From the vadose zone hydrology perspective at the landscape scale or larger, there is a need for simple and robust integration of surface remote sensing information into a dynamic soil water model in a distributed computing platform (e.g., geographical information systems [GIS]) to improve the simulation of root zone soil moisture.

For distributed models, GIS is considered the best available tool for organizing and processing data at the watershed/regional scale (Thielen et al., 1999; Lachassagne et al., 2001; Schreier and Brown, 2001; Renschler, 2003). A GIS stores spatial data, determines model parameters, provides scale-independent visualizations, and allows analysis and combination of maps from various scales (Thielen et al., 1999). Geographic information systems have influenced the development and implementation of hydrologic models in several different ways: (i) GIS has provided new opportunities to develop and run fully distributed models efficiently. These models take into account and predict the values of studied phenomena at any point within the watershed (Mitas and Mitasova 1998). (ii) GIS has also allowed users to run more traditional lumped models more efficiently and to include at least some level of spatial effects by partitioning entire watershed into smaller sub-watersheds. Hellweger and Maidment (1999) automated a procedure to define and connect hydrologic elements in ARC/INFO and ArcView and write the results to an ASCII file that is readable by the Hydrologic

Engineering Center's Hydrologic Modeling System (HEC-HMS). (iii) GIS has been used to transform what were originally site-specific models into spatially distributed models. (iv) GIS is sometimes used to vary model inputs and compare model outputs with field data for improving the scientific process understanding. Paniconi et al. (1999) reviewed the strengths and weaknesses of GIS and explained why distributed hydrologic models typically rely on GIS.

In this study we used the distributed modeling capability of GIS to apply a simple sequential data assimilation (i.e., EnKF) approach in conjunction with a numerically robust vadose zone hydrology model (i.e., HYDRUS-ET; Simunek et al., 1997) that incorporates periodic remotely sensed surface soil moisture observation (from a passive microwave remote sensor, ESTAR) to estimate root zone (profile) soil moisture. This newly developed soil moisture assessment tool (SMAT) has the advantage of combining the spatio-temporal continuity of the model prediction with intermittent input of remotely sensed observations in a geographically distributed framework to improve the root zone soil moisture estimation and minimize vadose zone model/parameter uncertainties using the data assimilation protocol.

## **Materials and Methods**

### ***Study Watershed and Distributed Hydro-Climatic Parameters***

The 603 km<sup>2</sup> Little Washita (LW) watershed (Fig. II-1) located in southwest Oklahoma in the Southern Great Plain (SGP) region of USA was selected for this study.

The LW watershed was chosen because it has been the focus of remote sensing experiments in 1992 Washita92 (Jackson et al., 1995), Washita94, SGP97 (Jackson et al., 1999), SGP99, and Soil Moisture Experiment 2003, SMEX03 (Jackson et al., 2005). Specifically, we used the ESTAR L-band passive microwave radiometer, horizontally polarized at 1.413 GHz (0.21 m) with a bandwidth of 20 MHz. ESTAR was used to map soil moisture at a resolution of 800 m X 800 m during the SGP97 experiment (Jackson et al., 1999). The detailed description of the SGP97 experimental plan and other supplementary information can be found at <http://hydrolab.arsusda.gov/sgp/sgp97>.

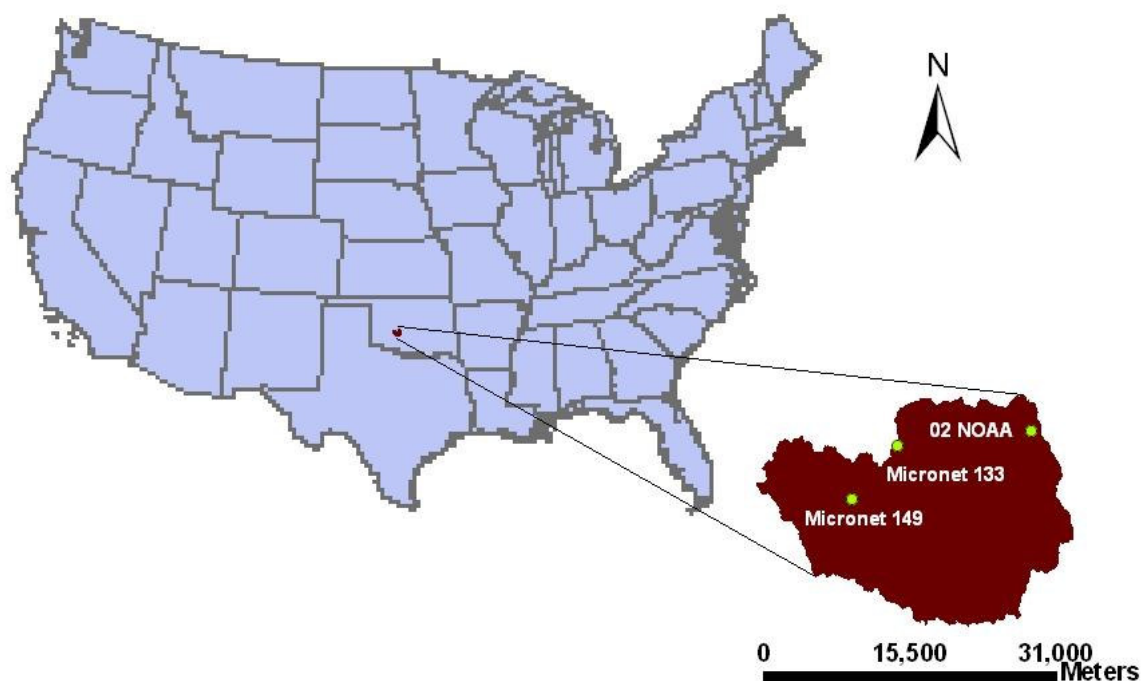


Fig. II-1. Little Washita (LW) watershed with Micronet and NOAA sites used in the study.



Extensive meteorological networks (of USDA-ARS Micronet, Oklahoma Mesonet, DOE/NOAA) across the region provide good spatio-temporal distribution of hydro-meteorological parameters. As used in this study, rain-gauges of USDA-ARS Micronet are strategically located in the watershed at a spacing of approximately 5000 m. Forty two of these stations continuously measure rainfall, solar radiation, air temperature, and relative humidity at 5-min intervals. At three stations, wind speed and barometric pressure are also recorded. There are 64 well-defined soil series in the LW watershed, with sand, loamy sand, sandy loam, loam, and silty loam being the predominant textures on the soil surface (Allen and Naney, 1991). Land use and land cover (LULC) is dominated by rangeland/pasture (63%) with significant areas of winter wheat and other crops mostly in the flood plains and western portion of the watershed. The topography of the region is moderately rolling with a maximum relief of less than 200 m.

All the relevant GIS data used in this study including soil properties, land cover, and remotely sensed surface soil moisture were derived from the SGP97 database available at [http://www.essc.psu.edu/nasa\\_lsh/](http://www.essc.psu.edu/nasa_lsh/). The meteorological data namely daily precipitation, wind speed, relative humidity, air temperature, and solar radiation used in this study were derived from <ftp://daac.gsfc.nasa.gov/data/sgp97/>. The footprint size of ESTAR-based soil moisture (800 m X 800 m) was used as the basis for grid resampling for all variables resulting in a total of 843 pixels across the LW watershed. The soil textural distribution (Fig. II-2) of LW has five dominant soil types: silty loam (32%), sandy loam (29%), loam (10.4%), sand (8.8%), and loamy sand (18%). During SGP97,

the LULC grid (Fig. II-3) had mainly four major land cover types: pasture, corn, wheat, and alfalfa. Average values of daily wind speed, relative humidity, and solar radiation based on all Micronet stations across the watershed were used for the model simulations. Micronet-based daily total precipitation data for the entire duration of SGP97 experiment (18 June 1997 to 16 July 1997) were spatially interpolated and resampled at 800 m X 800 m resolution.

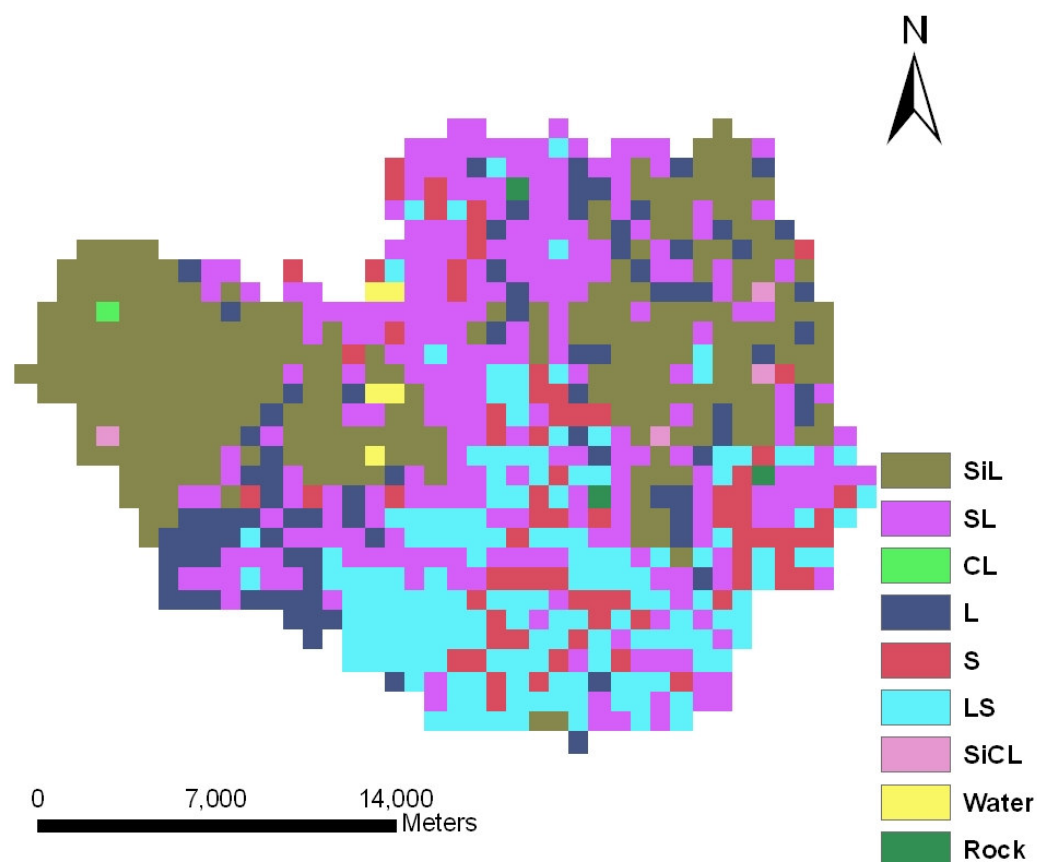


Fig. II-2. Little Washita (LW) watershed soil map resampled at a resolution of 800 X 800 m. (SL: sandy loam, SiL: silty loam, L: loam, CL: clay, LS: clay loam, S: sand, SiCL: silty clay loam).

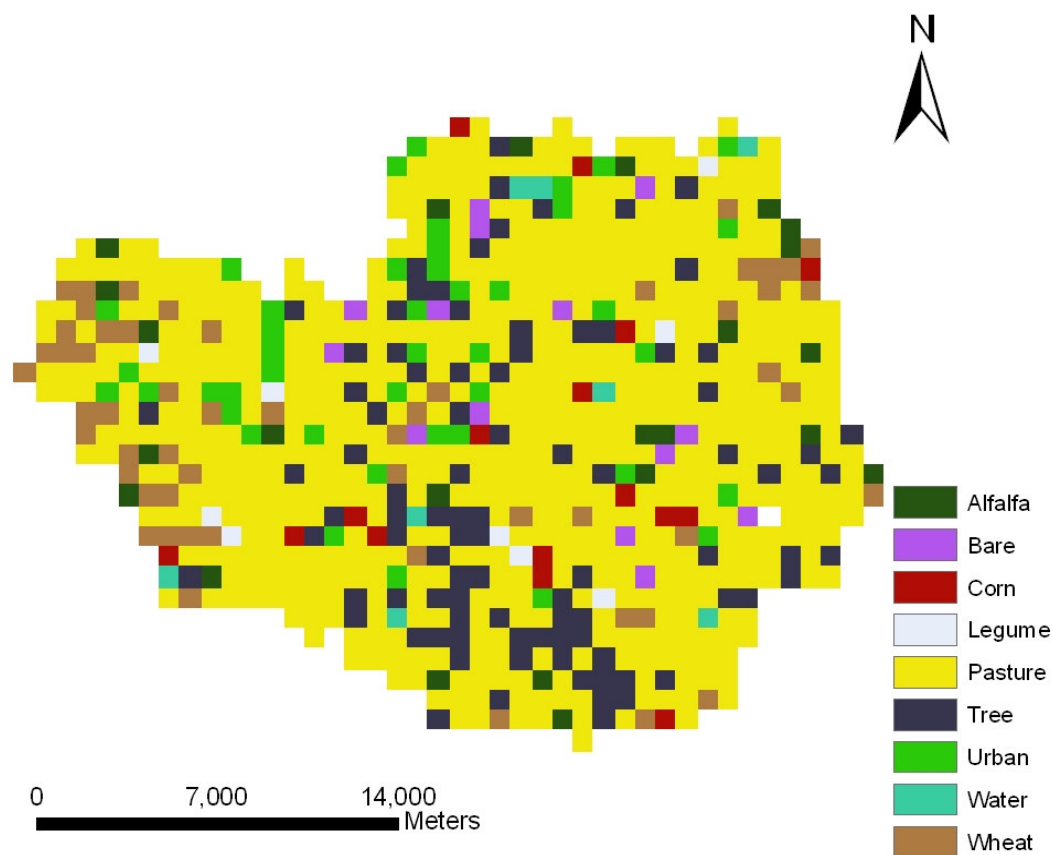


Fig. II-3. Landuse landcover (LULC) for Little Washita (LW) watershed resampled at a resolution of 800 X 800 m.

The resulting daily spatially-distributed hydro-climatic data sets were used as inputs to the HYDRUS-ET model. Other necessary distributed model inputs such as leaf area index, albedo, and surface roughness across the LW watershed were referred from Jackson et al. (1999). Knowledge of soil hydraulic properties is a key input for root zone/vadose zone hydrologic modeling. Laboratory and field methods for determining soil hydraulic properties across large land areas are time consuming and expensive. Average soil hydraulic properties based on soil texture (i.e., pedo transfer functions) are

commonly used in hydrologic models. In this study, the average values for selected soil water retention and hydraulic conductivity parameters for the major soil textural classes by Carsel and Parrish (1988) (Table II-1) were used. Local (point) profile soil moisture data measured at three Micronet sites (Heathman et al., 2003) highlighted in Fig. II-1 were used for comparison and validation with the model/data assimilation outputs at the pixel-scale.

Table II-1. Average hydraulic properties for different soil textures (Carsel and Parrish, 1988).

Texture	$\theta_r$	$\theta_s$	$\alpha$ (cm <sup>-1</sup> )	$n$	$K_{sat}$ (m d <sup>-1</sup> )
Sand	0.045	0.43	0.145	2.68	7.128
Loamy Sand	0.057	0.41	0.124	2.28	3.502
Sandy Loam	0.065	0.41	0.075	1.89	1.061
Loam	0.078	0.43	0.036	1.56	0.249
Silt	0.034	0.46	0.016	1.37	0.06
Silt Loam	0.067	0.45	0.02	1.41	0.108
Sandy Clay Loam	0.1	0.39	0.059	1.48	0.314
Clay Loam	0.095	0.41	0.019	1.31	0.062
Sandy Clay	0.1	0.38	0.027	1.23	0.028
Silty Clay	0.07	0.36	0.005	1.09	0.005
Clay	0.068	0.38	0.008	1.09	0.048

$\theta_r$ : residual water content,  $\theta_s$ : saturated water contents,  $\alpha$ , and  $n$  (-): fitting parameters related to particle-size distribution;  $K_{sat}$ : saturated hydraulic conductivity.

### ***Soil Moisture Assessment Tool (SMAT)***

The information flow for soil moisture assessment tool (SMAT) developed in this study to assess spatio-temporal distribution of profile soil moisture is presented in

Fig. II-4. The simplified distributed modeling system was primarily based on running the

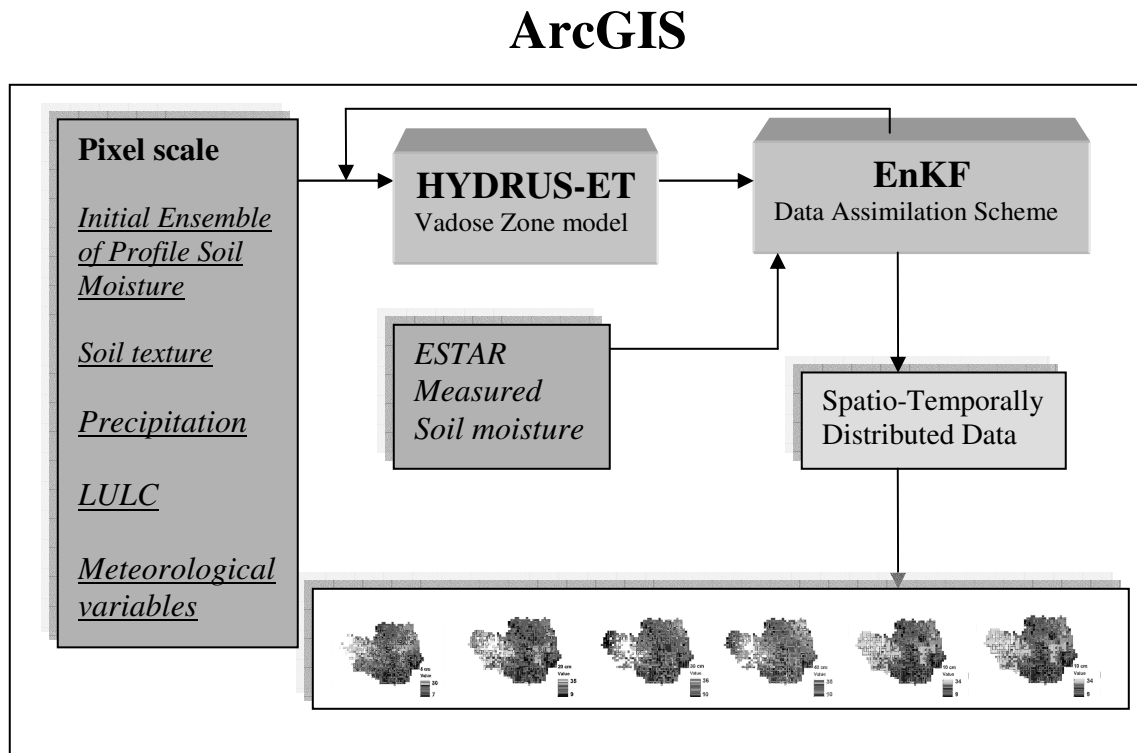


Fig. II-4. Schematic representation of the Soil Moisture Assessment Tool (SMAT).

one-dimensional partially-saturated vadose zone flow model HYDRUS-ET (Simunek et al., 1997) for each remote sensing footprint / pixel (800 m X 800 m) without any pixel-to-pixel interaction within the ArcGIS framework. A major advantage of this GIS-based tool is its capability to automatically read and write (I/O) the spatially distributed input data (e.g., soil, landuse-landcover, precipitation, and initial ensemble for each time step),

and execute the HYDRUS-ET model in every pixel. The toolbox also writes the mean results of the updated ensemble according to their geospatial coordinates.

We setup the one-dimensional HYDRUS-ET model for 843 ESTAR footprints/pixels across the LW watershed. The distributed footprint-scale parallel non-interacting stream tubes (soil columns/hydrologic units) were identified on a pixel basis with top/bottom boundary conditions, initial profile soil moisture conditions, and soil and land parameters. An interface program was developed in Microsoft Visual Basic 6.0 using Arc Objects to couple ArcGIS 9 with HYDRUS-ET and EnKF using a C subroutine (Dynamic Link Library). The integrated model reads pixel-wise input information (soil texture, landuse-landcover, precipitation) from the GIS grids and assigns parameters, boundary conditions, and initial conditions in the input files of HYDRUS-ET. Other specifications and assumptions for our model simulations runs are given in Table II-2. Soil profiles of 0.65-m thickness were considered with atmospheric top boundary and free draining bottom boundary. The soil profile was discretized into 97 elements (ranging from 0.001 m to 0.1 m) with finer discretization near the land-atmosphere boundary where a large hydraulic gradient was expected as compared to the deeper depths. Time dependent top boundary conditions were used with precipitation distribution across the LW watershed. A unit (vertical) hydraulic gradient (free drainage) condition was used at the bottom boundary of the root zone for all the pixels. In free drainage bottom boundary condition the discharge rate  $q(n)$  assigned to the bottom node is determined by the equation  $q(n) = -K(h)$ , where  $h$  is the local value of the pressure head, and  $K(h)$  is the hydraulic conductivity corresponding to this pressure head.

The spatial correlation of the uncertain initial soil profile input is unknown a priori and difficult to characterize. Porosity and wilting point control the upper and lower limit of volumetric soil moisture, respectively. The saturated hydraulic conductivity, which is highly variable in space, is a primary factor affecting infiltration. So, the initial status of soil moisture in the discretized soil profile is assigned a uniform value of 50% of the relative saturation according to soil type/texture. For computational limitations and efficiency 100 replicates were populated in the ensemble with a Gaussian noise of 20% to 5% of the soil moisture in decreasing order from top to bottom of the soil profile. Reichle et al. (2002) and Crow and Wood (2003) demonstrated with synthetic test problems that an ensemble of 100 replicates is sufficiently large to provide accurate estimates of soil moisture for the SGP conditions.

Due to lack of physical data, and for computational simplicity, we assumed: (i) only one soil texture per pixel for the entire root zone (soil texture at the soil surface was assigned for the whole depth of 0.65 m soil profile), (ii) pixel with rock outcrop, urban and water cover were excluded in the simulation, (iii) any excess water above the soil surface was immediately removed, and (iv) runoff and runoff between adjacent (800 m X 800 m) pixels due to surface topography was considered minimal thus limiting the flow in the vertical direction only.

Table II-2. Definition, values, and sources for the parameters used in HYDRUS-ET.

Parameter definition	Value
Number of soil layers	1
Thickness of soil zone	0.65 m
Soil hydraulic properties	Carsel and Parrish (1988)
Time step	Daily
Heat flow	Nil
Solute flow	Nil
Root growth	Nil
Upper boundary	Atmospheric
Bottom boundary	free drainage
Hysteresis	Nil
Number of Fixed nodes/elements across soil profile	97
Surface roughness	Jackson et al., 1999
LAI	Jackson et al., 1999
Transpiration depth of all land cover	0.6 m ( below top 0.05 m)
Wind speed	average wind speed of watershed
Ambience temperature	average temperature of watershed,
Relative humidity	average relative humidity of watershed

LAI: leaf area index.

To assess the performance of the integrated model (SMAT) we conducted a simulation experiment based on the dataset of SGP97 Hydrology experiment for LW watershed (Jackson et al., 1999). The SMAT was run for the entire duration of SGP97 remote sensing experiment ranging from Day of Year (DOY) 169 to 197 (18 June 1997 through 16 July 1997) for profile soil moisture estimation on a daily time step. The dates when (ESTAR) measured soil moisture were not available, model forecast ensemble estimates were carried forward with time for the entire profile. Availability of (ESTAR)



measured soil moisture to the model was made through analysis/update of the ensemble. Final state and measurement estimate are calculated by averaging the predictions made by the model replicates within the ensemble. After the completion of the data assimilation protocol for daily time-steps, ensemble means were written to an output file and read into soil moisture grids at various depths across the watershed.

### ***A Brief Description of HYDRUS-ET and Governing Equations***

HYDRUS-ET is a numerical model with a Galerkin-type linear finite-element scheme that solves the Richards' equation for partially saturated water flow. The one-dimensional water movement in a partially saturated rigid porous medium is described by a modified form of Richards' equation using the assumption that the air phase plays an insignificant role in the liquid-flow process and that the water flow due to thermal gradient could be neglected:

$$\frac{\partial \theta}{\partial t} = \frac{\partial}{\partial x} \left[ K \left( \frac{\partial h}{\partial x} + \cos \beta \right) \right] - S \quad \text{[II-1]}$$

where  $h$  is the soil water pressure head [m],  $\theta$  is the volumetric water content [ $\text{m}^3 \text{m}^{-3}$ ],  $t$  is the time [s],  $x$  is the spatial coordinate [m],  $S$  is the sink term [ $\text{m}^{-3} \text{s}^{-1}$ ],  $\beta$  is the angle between the flow and the vertical axis, and  $K$  is the unsaturated hydraulic conductivity function [ $\text{ms}^{-1}$ ] given by

$$K(h, x) = K_s(x) K_r(h, x) \quad \text{[II-2]}$$

where  $K_r$  is the relative hydraulic conductivity and  $K_s$  is the saturated hydraulic conductivity. The unsaturated soil hydraulic properties,  $\theta(h)$  and  $K(h)$ , generally highly

nonlinear functions of pressure head, were described by van Genuchten (1980):

$$\theta(h) = \theta_r + \frac{\theta_s - \theta_r}{[1 + (\alpha h)^n]^{1-\frac{1}{n}}} \quad [\text{II-3}]$$

where  $\theta(h)$  represents the water retention curve defining the water content,  $\theta$  ( $\text{m}^3/\text{m}^3$ ), as a function of the soil water pressure head  $h$  (m),  $\theta_r$  and  $\theta_s$  ( $\text{m}^3/\text{m}^3$ ) are residual and saturated water contents, respectively, while  $\alpha$  ( $\text{m}^{-1}$ ) and  $n$  (-) are fitting parameters related to particle-size distribution. Equation [II-3] is used in conjunction with the pore-size distribution model by Mualem (1976) to yield the hydraulic conductivity function (van Genuchten, 1980):

$$K(S_e) = K_o S_e^l \{1 - [1 - S_e^{n/(n-1)}]^{1-1/n}\}^2 \quad [\text{II-4}]$$

where  $K_o$  is the matching point at saturation (m/s), and parameter  $l$  (-) is an empirical pore tortuosity/connectivity parameter. The model considers prescribed water flux at the top and bottom boundaries across the root zone determined by atmospheric conditions or free drainage. The Penman method was used to calculate daily evapotranspiration using two steps: (i) calculate the potential evapotranspiration (PET) and (ii) calculate the actual evapotranspiration rate using a relationship between relative evapotranspiration and the pressure head,  $h$ , along the soil profile.

$$E/E_o = f(h) \quad [\text{II-5}]$$

The potential evapotranspiration,  $E_o$ , is calculated using the generalized method of Penman.

$$E_o = \frac{\phi(R_n - G_s) + \rho_a c_p (1/r_a) d'}{c_p + L\phi} \quad [\text{II-6}]$$

where  $E_0$  is the potential evapotranspiration rate,  $R_n$  is the average daily net radiation intensity,  $G_s$  is the heat flux into the soil,  $\rho_a$  is the air density,  $c_p$  is the specific heat capacity of the air at the constant pressure,  $r_a$  is aerodynamic resistance of evaporating surface, where  $\Phi = dm_0/dT$ ,  $m_0$  is the specific moisture content of air saturated with water vapor at  $T$  (temperature),  $L$  is the latent heat of evaporation and  $d'$  is the air saturation deficit. Novak (1987) formulation is used in HYDRUS-ET to calculate potential evaporation.

$$E_{e0} = E_0 \exp(-0.463 LAI) \quad [\text{II-7}]$$

where  $LAI$  is the leaf area index of the pixel. The potential transpiration,  $E_{t0}$  is

$$E_{t0} = E_0 - E_{e0} \quad [\text{II-8}]$$

The sink term 'S' in Eq. [II-1] is the volume of water removed from a unit volume of soil per unit time due to plant water uptake. Feddes et al (1978) defined  $S$  as

$$S(h) = \alpha(h) S_p \quad [\text{II-9}]$$

where  $\alpha(h)$  is the root water uptake water stress response function of the soil water pressure head ( $0 \leq \alpha \leq 1$ ) and  $S_p$  is the potential water uptake rate. The  $S_p$  is equally distributed over the entire root zone,

$$S_p = \frac{1}{L_R} E_{t0} \quad [\text{II-10}]$$

where  $E_{t0}$  is potential transpiration rate and  $L_R$  is the depth of the root zone.

### ***Ensemble Kalman Filter***

Data assimilation systems are typically designed to merge uncertain predictions

from models with incomplete and noisy measurements from an observing system. Assimilation approaches optimally combine model predictions and independent observations in such a manner that the shortcomings of each approach are mutually compensated. Evensen (2003) presented an algorithm based on ensemble of model predictions to evaluate error covariance information necessary for standard Kalman Filter (KF) for updating model predictions using observations. The method uses a nonlinear model to propagate the ensemble state across space or time. The initial ensemble was chosen to properly represent the soil profile error statistics by adding perturbation (Gaussian distributed noise) to the initial guess of the model states. The resulting ensemble reflects the uncertainty introduced by input errors. The ensemble replicates a broad range of values and the variances of the propagated states increase, as compared to the case where model input values are held fixed at their nominal values. This increased variability across the ensemble tends to make the filter rely more on measurements and reduces the adverse impact of model bias. We used an ensemble size of 100 in the application described here. It uses the physics of the vadose zone model (HYDRUS-ET) to vertically extrapolate surface soil moisture measurements to soil moisture states at deeper depths not directly observed by the remote sensor. The nonlinear one-dimensional vadose zone model used for assimilation can be represented in a generic form as the spatially discretized soil moisture at all computational nodes across the soil profile at time  $t$  into a state vector  $\psi$  of dimension  $n$  (Reichle et al., 2002):

$$\frac{d\psi}{dt} = F(\psi) + \omega \quad [\text{II-11}]$$

The nonlinear operator  $F(\cdot)$  include all deterministic forcing data (e.g., observed rainfall). Uncertainties related to the errors in the model or the forcing data are summarized in  $\omega$ . The observations used for the assimilation scheme are remotely sensed (ESTAR) measurements of soil moisture across the LW watershed during the SGP97 experiment (Jackson et al., 1999). The ensemble of model state is integrated forward in time according to Eq. [II-11]. The matrix of the forecast ensemble members can be written as:

$$A = (\psi_1, \psi_2, \psi_3, \dots, \psi_N) \in \mathfrak{R}^{n \times N} \quad [\text{II-12}]$$

where  $N$  is the number of ensemble members and  $n$  is the size of the model state vector.

The ensemble-mean matrix ( $\bar{A}$ ) can be defined as

$$\bar{A} = A 1_N \quad [\text{II-13}]$$

where  $1_N \in \mathfrak{R}^{n \times N}$  is a matrix in which each element is equal to  $1/N$ . The ensemble perturbation matrix can then be defined as

$$A' = A - \bar{A} \quad [\text{II-14}]$$

The ensemble covariance  $P_e \in \mathfrak{R}^{n \times n}$  can be defined as

$$P_e = \frac{A'(A')^T}{N-1} \quad [\text{II-15}]$$

For example, at time  $t_i$  over the region of interest, we possess an ensemble of forecasts that are representative of the true state of soil moisture. Typically, the ensemble-mean forecast is the best prediction of the profile soil moisture state at  $t_i$ . Now if we receive an ESTAR-based soil moisture observation at the same time  $t_i$ , then we need to update our

prediction of the soil moisture state and its uncertainty given this new observation. While the observation carries information about the surface soil moisture state only, we intend to extract information about the entire soil moisture profile. Thus, the representative forecast ensemble was used to derive polynomial coefficients between surface and subsurface computational nodes present in the state vector ( $A$ ) by using a least squares fit. These polynomials were then used to calculate the observed state vector of measurement ensemble by adding perturbation (Gaussian distributed noise). Given a vector of observation  $d$ ,

$$D = (d_1, d_2, d_3, \dots, d_n) \in \mathfrak{R}^{n \times N} \quad [\text{II-16}]$$

The perturbation matrix of  $D$  is defined by

$$X \in \mathfrak{R}^{n \times N} \quad [\text{II-17}]$$

from which we construct the ensemble of the covariance matrix

$$R_e = \frac{XX^T}{N-1} \quad [\text{II-18}]$$

The updated equation, expressed in terms of ensemble covariance matrices, is

$$A^a = A + P_e H^T (H P_e H^T + R_e)^{-1} (D - HA) \quad [\text{II-19}]$$

where  $A^a$  is the updated matrix,  $(D - HA)$  is the innovation matrix,  $P_e H^T (H P_e H^T + R_e)^{-1}$  is the Kalman gain, and  $H$  interpolates the true state (i.e., ESTAR based brightness temperature) of the observed quantity (i.e., soil moisture). In this case  $H$  is an identity matrix because the soil moisture product of ESTAR was used directly instead of microwave brightness temperature. The analyzed/updated matrix  $A^a$  is carried forward in time as ensemble of initial state for the next time step.

### ***Statistical Methods***

To evaluate the performance of the proposed data assimilation scheme with respect to the point measurements of profile soil moisture, we used coefficient of determination ( $R^2$ ), root mean square error (RMSE), and mean bias error (MBE). The statistics of RMSE and MBE are defined as

$$RMSE = \sqrt{\frac{\sum (P - O)^2}{n}} \quad \text{[II-20]}$$

$$MBE = \frac{\sum (P - O)}{n} \quad \text{[II-21]}$$

where  $P$ ,  $O$  are predicted and observed soil moisture, respectively, and  $n$  is the number of observations. The root mean square error and MBE are indicative of overall error and mean bias in the estimation process, respectively.

## **Results and Discussion**

Performance of the SMAT was evaluated by comparing the simulated (overlapping) footprint-scale profile soil moisture to the local (point-scale) profile soil moisture data measured at three Micronet sites (Heathman et al., 2003) highlighted in Fig. II-1. These three sites (i.e., Micronet-133, Micronet-149 and 02-NOAA) were selected for validation because they represent typical scenarios in the LW watershed.

### ***Site Micronet-133***

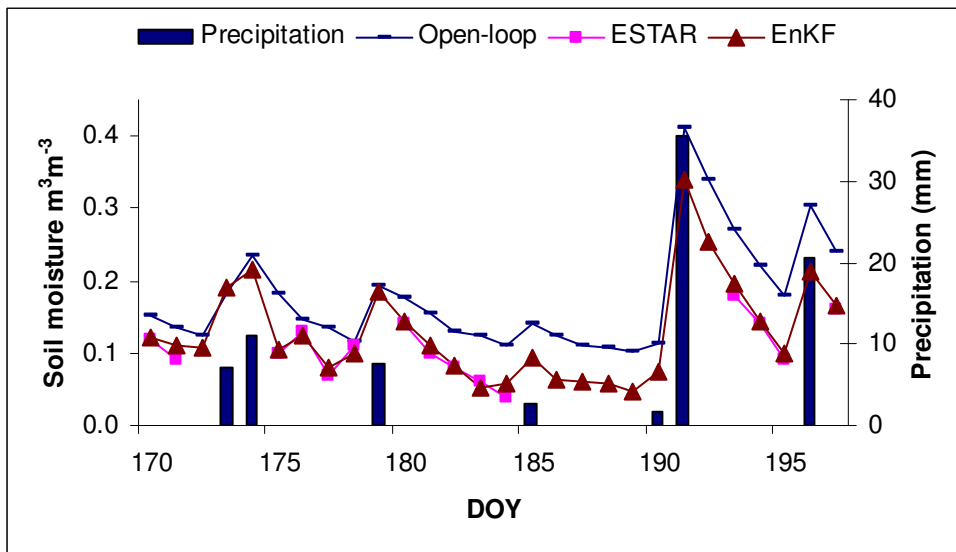
Site Micronet-133 was selected due to the matching soil profile (based on pixel-scale NRCS soil database, Fig. II-2) used in the model and the local (point-scale) observation at the field site. Point observations indicate a sandy loam soil for the entire soil profile, which agrees with our model assumption of the soil texture at the soil surface assigned for the whole soil profile depth of 0.65-m. Figure II-5a shows the surface soil moisture comparison between models without data assimilation (Open-loop) and with EnKF-based data assimilation, and ESTAR observations at the top 0-5 cm depth. Open loop results are obtained from the average of 100 replicates without updating. Figure II-5a illustrates the ability of EnKF to correct the errors in HYDRUS-ET model.



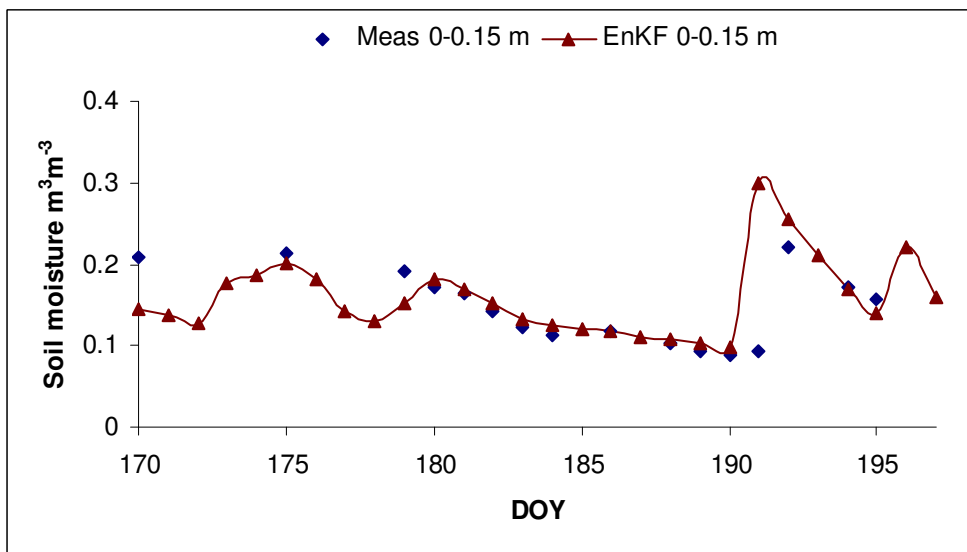
Table II-3. Comparison of field soil moisture measurements and model results from Day of Year (DOY) 170 to 197 at 02-NOAA, Micronet-133, and Micronet-149.

Sites	Statistics	0-0.15 m	0.15-0.30 m	0.30-0.45 m	0.45-0.60 m
Micronet-133	Local	SL	SL	SL	SL
	Model	SL	SL	SL	SL
	R <sup>2</sup>	0.82	0.84	0.88	0.79
	MBE	-0.0052	0.0014	-0.007	0.01
	RMSE	0.0048	0.0057	0.0002	0.002
Micronet-149	Local	SiL	SiL	L	CL
	Model	SiL	SiL	SiL	SiL
	R <sup>2</sup>	0.81	0.67	0.25	0
	MBE	0.0029	-0.0715	-0.0847	-0.1129
	RMSE	0.012	0.0065	0.0261	0.0392
02-NOAA	Local	L	Cl	L	SiL
	Model	SL	SL	SL	SL
	R <sup>2</sup>	0.55	0.3	0.23	0.15
	MBE	-0.1034	-0.1674	-0.1697	-0.1697
	RMSE	0.0174	0.0342	0.0394	0.0398

SL: sandy loam, SiL: silty loam, L: loam, Cl: clay, CL: clay loam.

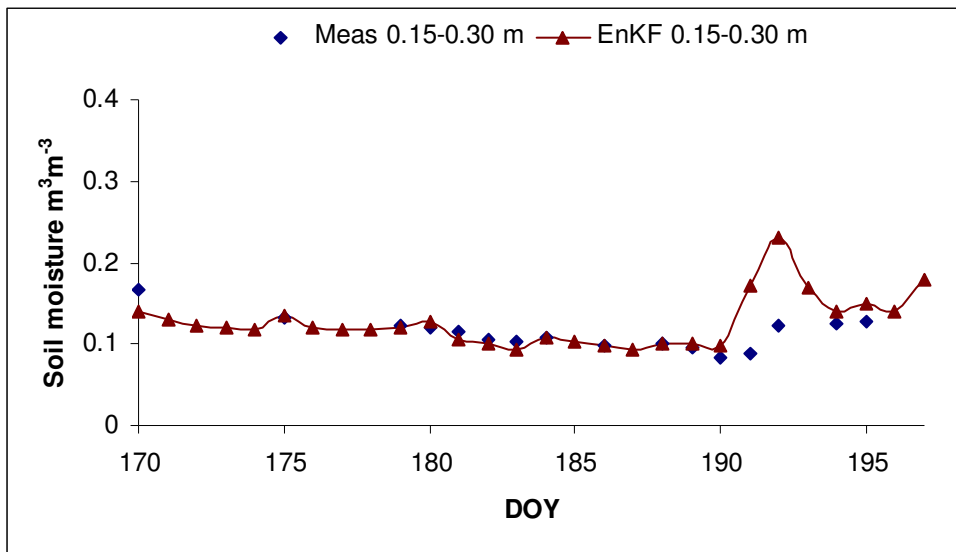


(a)

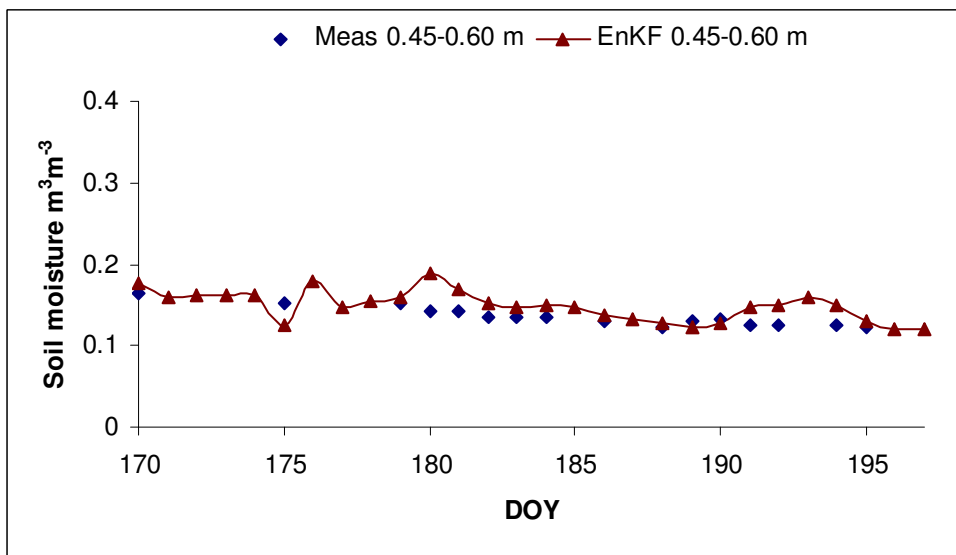


(b)

Fig. II-5. Site Micronet-133 temporal series of soil moisture at a) surface, b) 0-0.15 m, c) 0.15-0.30 m, and d) 0.45-0.60 m. (DOY: day of year, EnKF: ensemble Kalman filter, Meas: Measured).



(c)



(d)

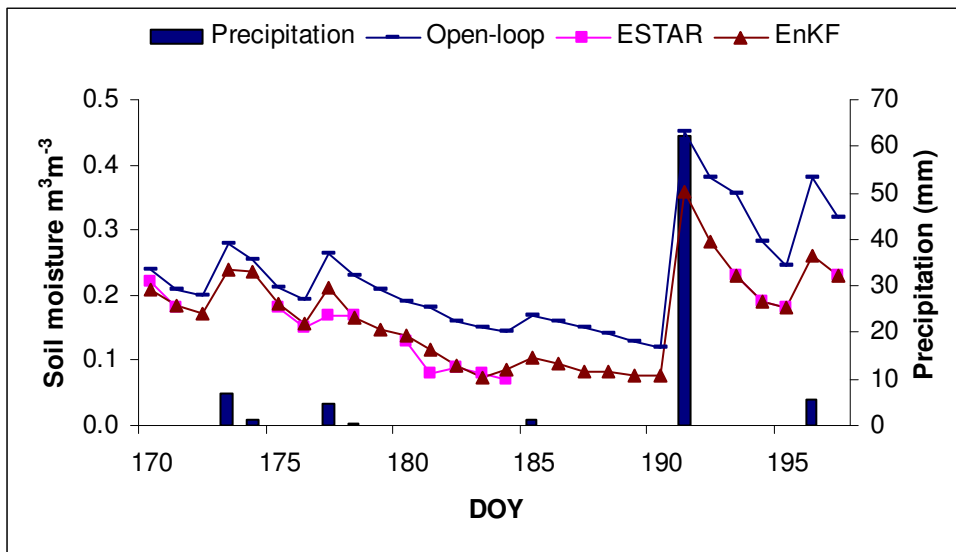
Fig. II-5. Continued.

Figures II-5b-d show the comparison of SMAT-based profile soil moisture estimations and TDR-based field observations at four different depths. From DOY 170 to 175 the

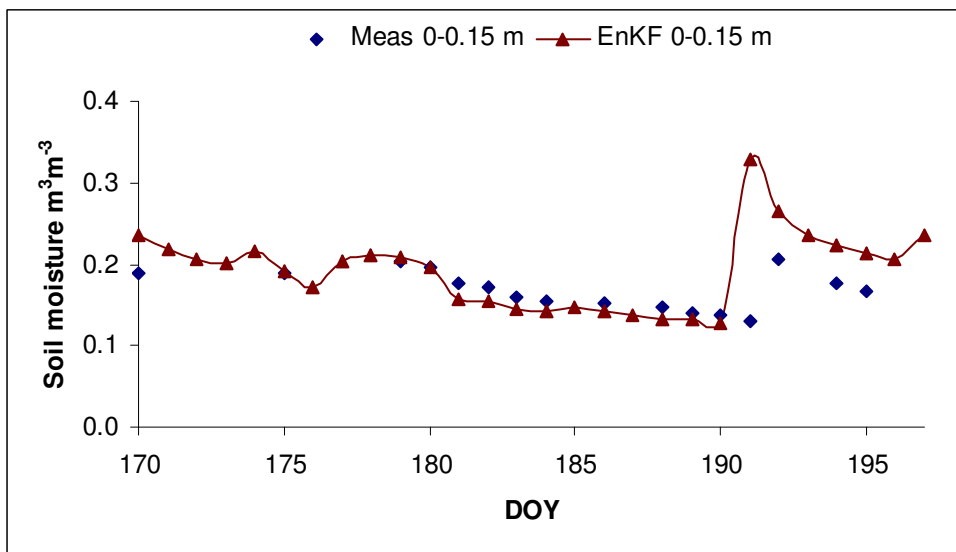
root zone soil moisture estimated by the model at the depths of 0-0.15 m, 0.15-0.30 m, and 0.45-0.60 m depends on the initial estimate of the ensemble. The filter improved the surface soil moisture at the initial period of the simulation, in contrast to the soil moisture at the deeper depths. The continuous analysis/update (i.e., EnKF-based assimilation of surface soil moisture using ESTAR observations) from DOY 175 to 184 (except on 179) improved the profile soil moisture estimations and the trends of the simulated and observed states matched well. These matching trends in Fig. II-5b-d verify the hypothesis that surface soil moisture observation obviously carries information in the memory about the unobserved portion of the state (profile soil moisture). Even after the gap in ESTAR over-flights between DOY 184 to 192 the model maintains a good trend except on DOY 191. On DOY 191, the impact of a rainfall event is clearly visible in the model estimates, but was missing in the measured soil moisture at the depth of 0-0.15 m (Fig. II-5b). This emphasizes the importance and sensitivity of the precipitation information available to the model at a daily time step, which affects the performance of the model. The filter regained the trend from DOY 193 due to new ESTAR measurements from DOY 193 to 197 except on 196. Statistical comparison of the model estimations with point measurements is given in Table II-3. For this site high  $R^2$  values were observed for all the depths across the root zone indicating the efficient data assimilation capability of SMAT for surface soil moisture reaching to the deeper depths under favorable conditions (i.e., for matching soil profile at the pixel- and point-scales). Low RMSE values observed for this site confirm the suitability of the model and agreement of assumptions with field conditions.

### ***Site Micronet-149***

The actual soil profile (based on point observations) of this site matches the model soil profile of silty loam for the top 0.30 m (Table II-3). Figure II-6a shows the surface (0-5 cm) soil moisture comparison among the Open-loop, model with EnKF, and ESTAR observations. As expected the Open-loop and EnKF predictions drift apart, and ESTAR measured soil moisture allow the EnKF to capture the dry-down portion of the experiment (DOY 170 to 185). Uncertainty in hydraulic parameters and bottom boundary condition and the mismatch of soil profile below 0.30 m were the limiting factors for the model. The bottom-most clay layer in the actual soil profile restricted the downward flux during the experiment and retained higher moisture in the soil profile between the depths of 0.30 to 0.60 m. The higher  $K_s$  value of silt loam (Table II-1) than clay loam layer considered in the model drained the soil profile faster during the simulation resulting in lower soil moisture predictions. The EnKF algorithm failed to maintain the temporal trends at the deeper layers (except the surface moisture) due to imperfect forecast ensemble polynomial coefficients obtained by least squares fit. Figures II-6b-d illustrate the comparison of profile soil moisture using the data assimilation scheme (SMAT) and field observed values at the depths of 0-0.15 m, 0.15-0.30 m, and 0.45-0.60 m. Of particular significance, the EnKF estimates for soil profile at the 0-0.15 m depth closely matched the point-scale measurements (Fig. II-6a) with  $R^2$ , MBE, and RMSE values of 0.81, 0.0029, and 0.01, respectively (Table II-3).

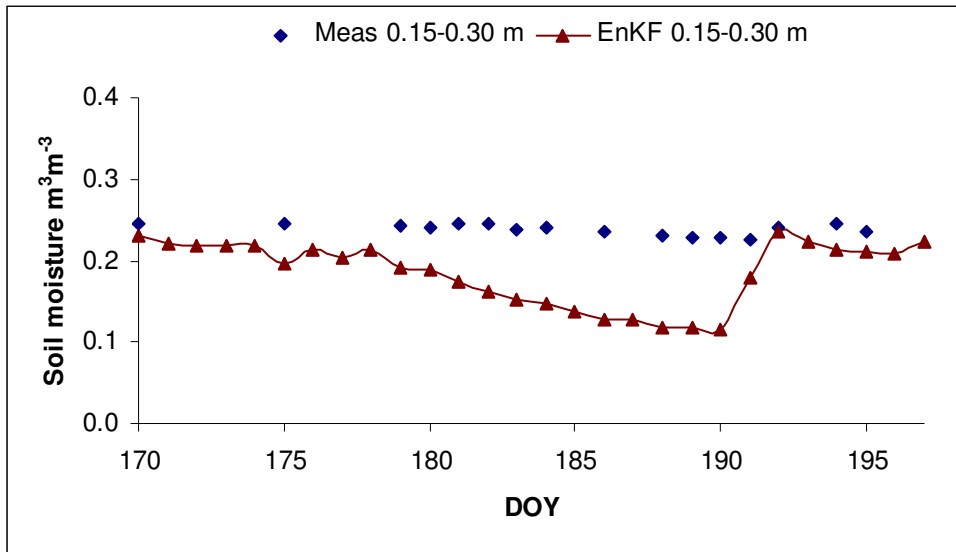


(a)

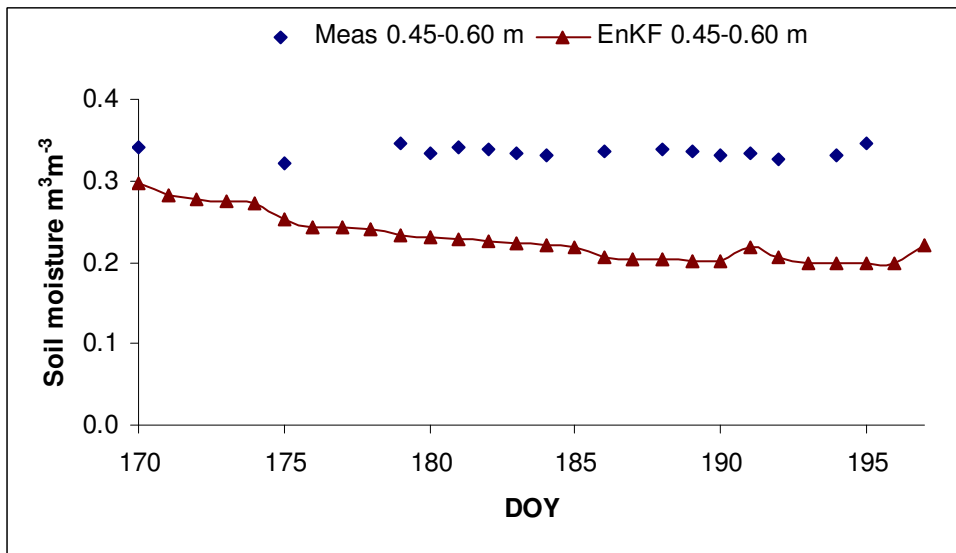


(b)

Fig. II-6. Site Micronet-149 temporal series of soil moisture at a) surface, b) 0-0.15 m, c) 0.15-0.30 m, and d) 0.45-0.60 m. (DOY: day of year, EnKF: ensemble Kalman filter, Meas: Measured).



(c)



(d)

Fig. II-6. Continued.

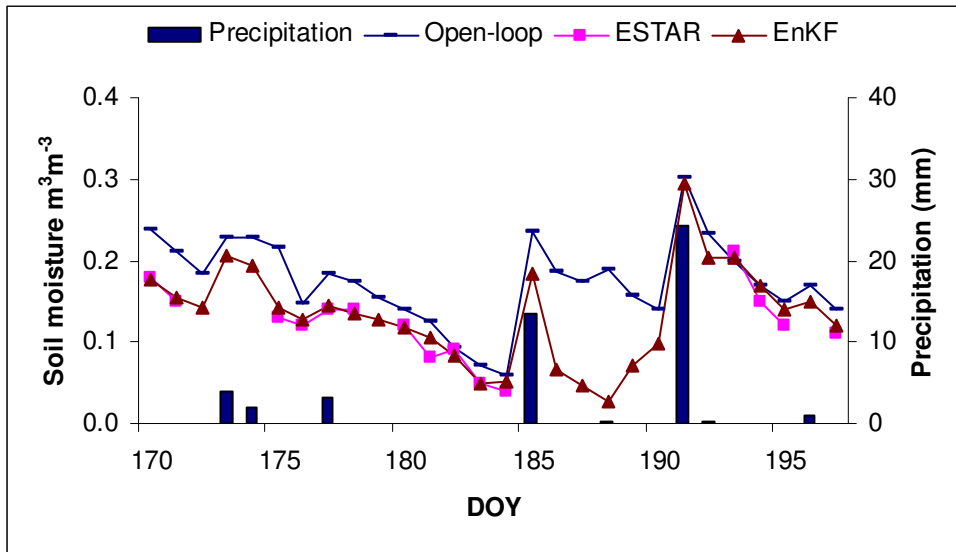
Even though the profile soil texture at the 0.15-0.30 m depth in the model and at the field location were the same, observed and estimated soil moistures at this depth did not

match well (see Fig. II-6c) due to the impact of the clay loam layer at the bottom of the profile. The filter totally underestimated the soil moisture in the deeper zone 0.45-0.60 m with a MBE of -0.1129 (Table II-3). At the field site, however, the clay layer retains moisture at an average  $0.35 \text{ m}^3/\text{m}^3$  throughout the observation period due to the impeding layer.

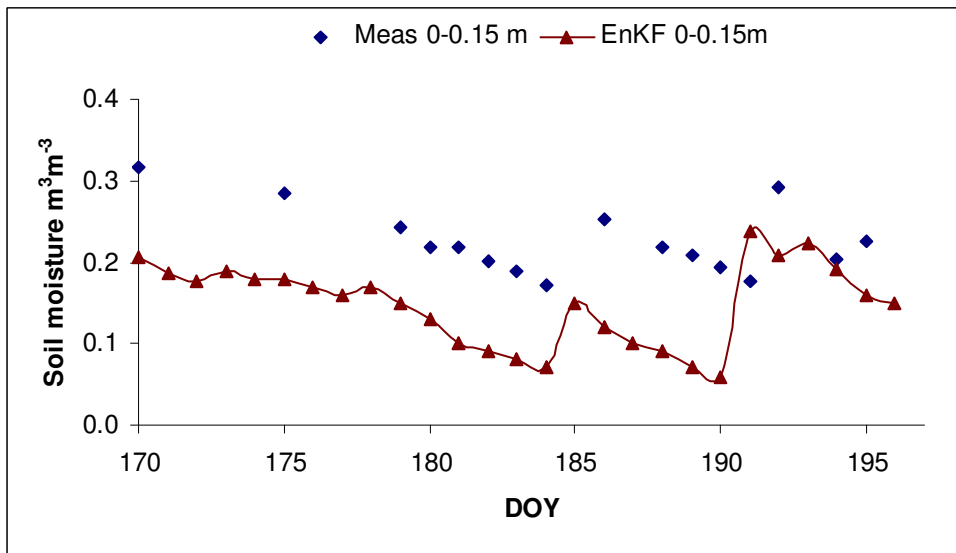
### ***Site 02-NOAA***

This site was especially chosen to demonstrate the impact of a total mismatch of the model soil profile with the local soil profile (Table II-3), which completely alters the flow regime of the soil column by introducing uncertainty in hydraulic parameters. The model used sandy loam for the entire 0-0.60 m soil profile, which led to a well-drained soil column for this site. Neither the Open-loop nor the EnKF could predict the local soil moisture at this site. As evident from Figs. II-7b-d, no agreement between measured and EnKF was observed at any depth, with high negative bias for the entire root zone (Table II-3). Note, however, EnKF could update the surface (0-5 cm) soil moisture prediction across the study period (Fig. II-7a). A partial agreement was observed at the depth of 0-0.15 m following the rainfall event on DOY 191.



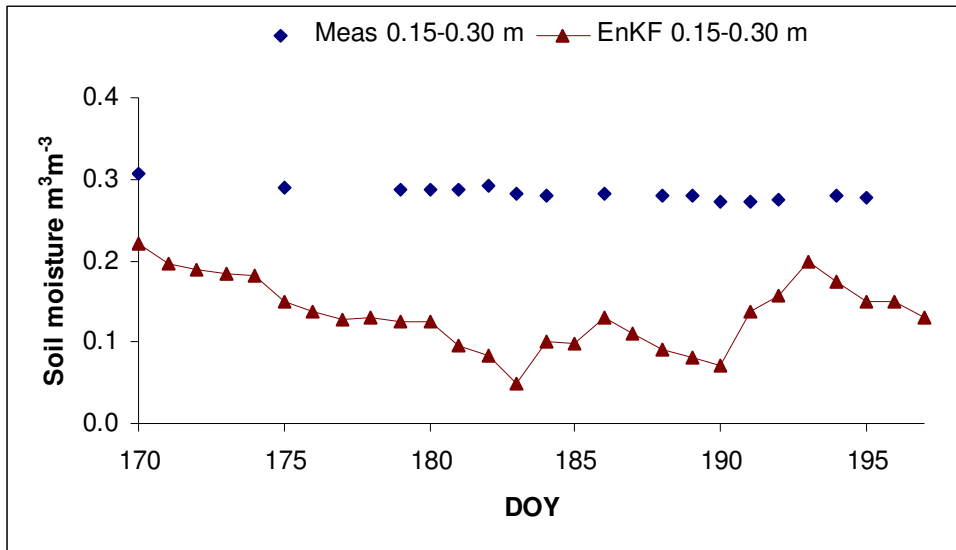


(a)

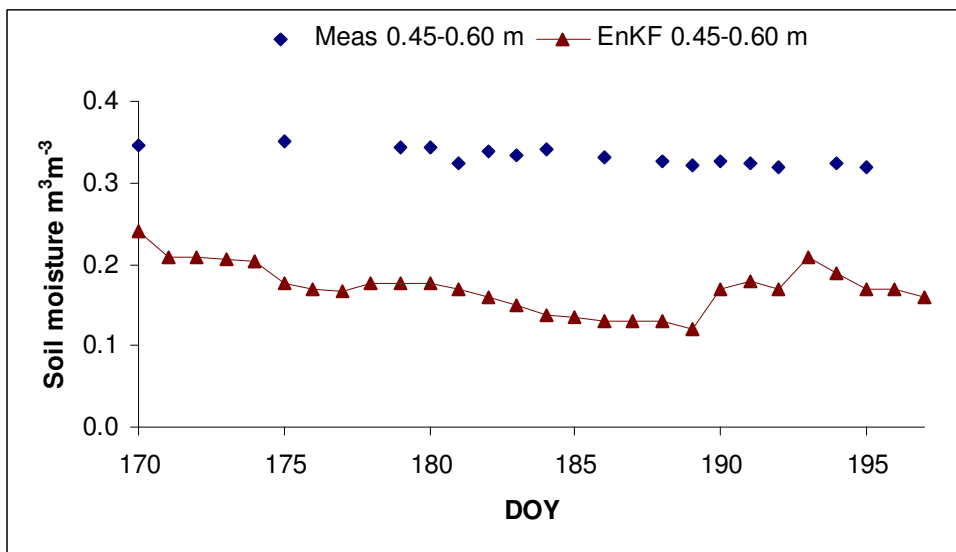


(b)

Fig. II-7. Site 02-NOAA temporal series of soil moisture at a) surface, b) 0-0.15 m, c) 0.15-0.30 m, and d) 0.45-0.60 m. (DOY: day of year, EnKF: ensemble Kalman filter, Meas: Measured).



(c)



(d)

Fig. II-7. Continued.

The duration of the SGP97 hydrology experiment was comparatively shorter than what is generally applied to models. It is not apparent whether a shorter period had any

appreciable effect on the model results, although some previous studies have found that soil moisture predictability may be related to the model time-scale (e.g., Schlosser and Milly, 2000). At all three study sites (02-NOAA, Micronet-133, and Micronet-149), in the early part of the experiment (first 10 days), EnKF estimated soil moisture on the surface was only marginally better than the Open-loop (see Fig. II-5a, II-6a, II-7a). Margulis et al. (2002) found similar results at the watershed/regional scales. For sites Micronet-133, Micronet-149, and 02-NOAA, Open-loop and EnKF for soil surface lead to RMSE of 0.062, 0.090, 0.054 and 0.010, 0.013, 0.011, respectively. Figures II-5a, II-6a, and II-7a confirm that EnKF is able to track the dry-down period after precipitation events much better than the Open-loop modeling scheme. A significant benefit of the EnKF in the proposed integrated model is its ability to instantaneously update moisture estimates and error standard deviations throughout the soil profile. This is possible due to the carry over memory of the surface soil moisture about the profile soil moistures. As discussed for the site Micronet-133, the effects of surface moisture update on the profile soil moistures only get evident gradually with time, as surface moisture variations redistribute throughout the soil profile (Figs. II-5b-d).

Precipitation is the most important time-dependent forcing data for soil moisture distribution in hydrologic studies (Margulis et al. 2002). Precipitation uncertainties, especially in ungauged areas, can be expected to have significant impact on the evolution and distribution of soil moisture. A major limitation of the integrated data assimilation model (SMAT) is the implications of deterministic forcing data, mainly precipitation. At the three study sites (02-NOAA, Micronet-133, and Micronet-149), the

peak surface soil moistures were observed after a day from the model estimation peak on DOY 191. This lagged behavior in surface soil moisture could partially be due to the use of daily (24-h cumulative) precipitation values reported for the following day. Subsequently, lagging surface soil moisture adversely affects the filter performance when comparing the results with the local point profile data for a particular day. Another limitation that affects the model performance of EnKF is the assumption of one soil texture across the whole depth of the soil profile. Soil hydraulic parameters for sandy loam and silty loam profiles of sites 02-NOAA and Micronet-149, respectively, in the model are much different from the local soil profiles. Furthermore, the spatial variability of soil hydraulic conductivity and soil water retention characteristics across the corresponding (ESTAR) remote sensing pixel greatly influence the vertical and lateral soil moisture transmission. The effect of soil texture was further illustrated by Mohanty and Skaggs (2001) who demonstrated the relationship of soil texture in determining soil moisture stability and variability across time at selected ESTAR remote sensing footprints during the SGP97 experiment. Inclusion of more detailed soil database or aggregated/effective soil hydraulic parameters (e.g., Zhu and Mohanty, 2002, 2003a, 2003b) for future applications of this distributed root zone soil moisture assessment tool (SMAT) may overcome this limitation.

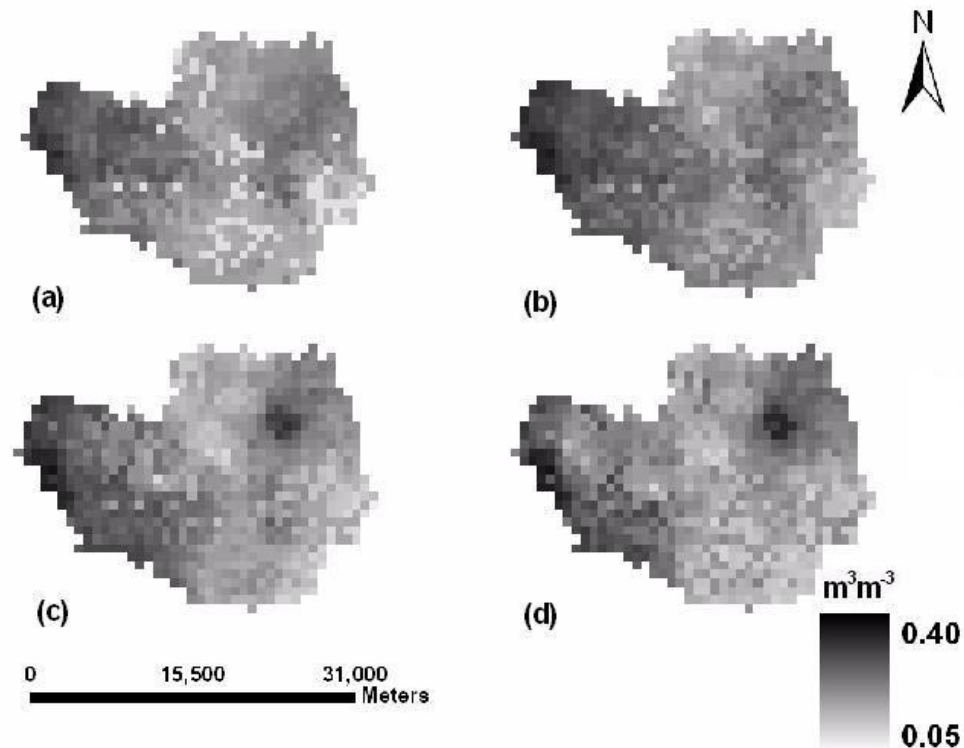


Fig. II-8. Model predicted soil moisture grids at different depths across Little Washita (LW) watershed Day of Year (DOY)193 (12<sup>th</sup> July 1997) at the depth of (a) 0.05 m, (b) 0.2 m, (c) 0.4 m and (d) 0.6 m.

Figure II-8 shows the output of our ArcGIS-based distributed root zone process model with the EnKF data assimilation scheme (SMAT) in terms of soil moisture states across the LW watershed for DOY 193 (12 July 1997) at four discrete depths (viz, 0.05 m, 0.20 m, 0.40 m, and 0.60 m). The discussion of Sellers et al. (1995) about spatial heterogeneity introduced by rainfall and removed through dry-down dynamics is also applicable at this coarse (watershed) scale. During the dry-down period, the effect of soil texture (Fig. II-2) on surface (0-5 cm) soil moisture patterns (Fig. II-8) is visible at this

scale, which matches with the findings of remote sensing observations across the SGP97 region (Jackson et al., 1999). A significant advantage of the ArcGIS-based SMAT is that it can be adopted at any fine or coarse spatial resolution to identify the transitional scale that separates (nonlinear) fine versus coarse scale soil moisture dynamics, where changes in soil moisture spatial heterogeneity are negatively or positively correlated with the change in mean soil moisture.

### **Conclusion**

We developed a new distributed root zone soil moisture assessment tool (SMAT) on the ArcGIS platform by fully integrating a one-dimensional vadose zone hydrology model (HYDRUS-ET) with EnKF data assimilation capability using the parallel non-interacting stream tubes concept and remotely-sensed surface soil moisture as the primary input. A major advantage of this novel scheme is that it can be used to compute root zone soil moisture distribution and its temporal evolution at multiple spatial resolutions including landscape, watershed, and regional scales. Results illustrate both the challenges and potential benefits of this new model. The system described here is formulated with its ultimate application in purview, i.e., operational estimation of near surface and root zone soil moisture using aircraft-/satellite-based microwave remote sensing measurements at different scales. Comparisons of EnKF filter simulations estimates with Open-loop simulations estimates also demonstrate the advantage of assimilating remote sensing measurements with model estimations, which are consistent

with previous studies at the SGP sites. Passive microwave-based soil moisture measurements are particularly important during the dry-down period when Open-loop model may diverge. The model displayed a reasonable capability to generate soil moisture distribution at the desired resolution at various depths of the root zone in Little Washita watershed during the Southern Great Plains 1997 (SGP97) remote sensing experiment. To improve model performance several issues need to be addressed in the future including 'effective' hydraulic parameters across spatial scales, developing subsurface soil properties data bases using direct and indirect methods, implementing more appropriate vadose zone flow models at landscape scale, correction of forcing data, and implementation on spatially correlated pixels.

## CHAPTER III

### SCALING OF SURFACE SOIL MOISTURE FIELDS DURING SMEX02

In this study, we examined the scaling properties of the Polarimetric Scanning Radiometer (PSR)-based remotely sensed soil moisture fields during the Soil Moisture Experiment 2002 (SMEX02) hydrology campaign using wavelet-based multiresolution analysis. The multiresolution technique decomposed the PSR-based soil moisture fields into large-scale average soil moisture fields and fluctuations in horizontal, diagonal and vertical directions at various resolutions. Results suggested linearity in the log-log dependency of the variance of soil moisture up to a resolution of 6100 m X 6100 m on PSR sampling dates during the SMEX02. The wet fields (with high soil moisture) show almost similar variance for all the resolutions signifying the strong spatial correlation. Analysis of the dry fields (with low soil moisture) indicated a log-log linearity of moments with various scales, and a concave functional relationship with the order of moments, typically representing a multiscaling process. The scaling exponent of soil moisture during drydown suggest a transition from simple scaling (in wet fields) to multiscaling (in dry fields) behavior. The detail components of multiresolution analysis in the horizontal and the vertical directions for dry and wet fields exhibited similarity, whereas the diagonal component shows difference in simple scaling properties. Another important finding of this study is the increase of subpixel soil moisture variability with increasing resolution, especially for the wet fields.



## Introduction

Soil moisture is highly variable across space scales of few meters to kilometers and time scales of minutes to months. The spatio-temporal scaling of soil moisture is influenced by non-linear soil moisture dependent processes (hydrological, meteorological and soil physical processes) (Western et al., 2003). Most of the hydrological and meteorological models involving soil moisture are nonlinearly parameterized and sensitive to spatio-temporal variability and scale dependency of soil moisture. Spatial scaling of soil moisture is poorly understood because it is difficult to model and measure in a comprehensive manner (Dubayah et al., 1997). However, airborne passive microwave remote sensing offers techniques to estimate soil moisture in top 5 cm of the soil surface over a large area with good spatial resolution (Jackson 1993). The operational constraint of airborne passive microwave remote sensing is that it can not achieve large spatial soil moisture fields on a routine basis. Recent deployment of space-borne sensor as AMSR-E has the capability to map soil moisture in large land areas on regular (1.5 days) intervals. In the foreseeable future, no space-borne passive microwave remote sensing platform will have ground spatial resolution finer than 40 km (Crow et al., 2005). Within such a coarse resolution (>40 km), great degree of soil moisture variability is observed over a large range of spatial scales encompassing various soil types, topographic features, vegetation and climatic conditions. Air-borne remote sensing campaigns including Washita '92 (Jackson et al., 1995), Washita '94, Southern Great Plains 1997 (SGP97) hydrology experiment (Jackson et al., 1999), SGP99, SMEX02 (Bindlish et al., 2005), SMEX03 (Jackson et al., 2005), SMEX04, and

SMEX05, provided us the unique opportunity to study the spatial scaling of soil moisture in variety of hydro-climatic conditions, within the coarse resolution of space-borne passive microwave remote sensing platform.

The soil moisture patterns (distributions) evolves from many different geophysical processes acting over different scales, such as topography, rainfall, soil characteristics and vegetation distribution (Dubayah et al., 1997). Past studies of these geophysical processes such as rainfall (Gupta and Waymire, 1990; Kumar and Foufoula-Georgiou, 1993a, 1993b), stream flow (Gupta and Waymire, 1990; Rodriguez-Iturbe et al., 1994), and clouds (Tessier et al., 1993) have suggested multiscaling properties. Rodriguez-Iturbe et al. (1995) studied and characterize the spatial pattern of soil moisture, and concluded that the variance of soil moisture follow a power law decay, typical of scaling processes, as a function of area over which soil moisture is observed. Hu et al. (1998) used multiresolution analysis to investigate the scale variation of soil moisture by decomposing soil moisture images into average large-scale and detailed small-scale fluctuation components. They found that average large-scale soil moisture was non-stationary at the scale studied (30 m to 10 km) and the small-scale fluctuations exhibited simple scaling process, while the overall soil moisture variability exhibited multiscaling properties. Kumar (1999) used estimation techniques based on multi-resolution tree to characterize the subgrid variability of soil moisture at multiple scales by combining information, such as soil moisture measurements and soil hydrologic properties available at different scales. Western and Blöschl (1999) examined the effect on the apparent spatial statistical properties of soil moisture (variance and correlation

length) on changing the measurement scale in terms of spacing (distance between samples), extent (overall coverage), and support (integration area). They found that the effect of extent on the correlation length is the most important one of the three (extent, support, and spacing). The apparent variance increases with the increasing extent, decreases with increasing support and does not change with spacing. Cosh and Brutsaert (1999) showed that grouping soil by textural class was useful to characterize the soil moisture field and their dynamics into groups with different statistical properties.

Famiglietti et al. (1999) used Electronically Scanned Thinned Array Radiometer (ESTAR)-based soil moisture data of SGP97 and point soil moisture measurements in selected fields to investigate within pixel variability of remotely sensed soil moisture. Mohanty and Skaggs (2001) also used ESTAR dataset of SGP97 to show the characteristic differences in the space-time dynamics of soil moisture within several remote sensing footprints with various combinations of soil texture, slope and vegetation type. They also found that ESTAR footprint average soil moisture matches differently with ground-based soil moisture reflecting nonlinearity in the hydrologic processes for various combinations of soil, topography, and land cover. Using measured and modeled soil moisture from Washita'92 and Washita'94 experiments Peters-Lidard et al. (2001) found multiscaling properties. Nykanen and Foufoula-Georgiou (2001) scaling study of soil moisture disagreed with the results of Rodriguez-Iturbe et al. (1995) and Hu et al. (1997) who reported log-log linear relationships of the variance of soil moisture with scale. More recently, Oldak et al. (2002) studied the statistical properties of remotely sensed soil moisture field (passive microwave remote sensing with ESTAR L-band

radiometer) of Washita '92 and SGP97 experiment. They found that the shape of scaling dependencies remains the same during drydown, consequently reducing the volume of observations needed to predict scaling of surface soil moisture during drydowns. Brunsell and Gillies (2003) conducted multiresolution analysis on radiometric temperature data of AVHRR (Advanced Very High Resolution Radiometer) and reported that at very large scales, statistical self-similarity was observed through all levels of aggregation. Studies at larger scales (50–1000 kms) (Vinnikov and Robock, 1996; Entin et al., 2000) from agricultural sites in the former Soviet Union, Mongolia, China, and the USA have found the soil moisture variation could be represented as a stationary field with a correlation length of 400-800 kms.

All aforementioned studies provide enough evidence that spatial scaling of soil moisture generally depend on topography, rainfall, soil characteristics and vegetation distribution. In this study, we examined the scaling properties of the Polarimetric Scanning Radiometer (PSR)-based remotely sensed soil moisture fields during SMEX02 hydrology campaign in Iowa. We focused on spatial scaling properties of soil moisture in the top soil layer (0-5 cm) of a region with high row crop agriculture. Wavelet based multiresolution techniques was used to decompose the soil moisture fields into large-scale average soil moisture fields and fluctuations in horizontal, diagonal and vertical directions at various resolutions. The primary objective of this study is to relate soil moisture variability at the scale of the PSR footprint (800 m X 800 m) to larger scale average soil moisture field variability. We also investigated the scaling characteristics of fluctuation fields among various resolutions.

## Materials and Methods

### *Study Region*

The regional study area of SMEX02 in Iowa is shown in Fig. III-1 (Bindlish et al., 2005). The details of SMEX02 experiment plan can be found at website ([hydroloab.arsusda.gov/SMEX02](http://hydroloab.arsusda.gov/SMEX02)). The duration of the study was from June 6<sup>th</sup> to 12<sup>th</sup> July 2002. Nearly 95% of the regional study area is used for row crop agriculture. Corn and soybean are grown on approximately 90% of the row crop acreage (in 2002, nearly 60% crop was corn and 40% soybean). The climate of SMEX02 regional site is humid, with an average rainfall of 835 mm. The regional site is considered as the pothole region of Iowa because of its undulating terrain (Bindlish et al., 2005). The PSR (Polarimetric Scanning Radiometer) observations were conducted during June 25<sup>th</sup> to July 12<sup>th</sup>, 2002. The PSR is an airborne microwave imaging radiometer operated by NOAA Environmental Technology Laboratory (Piepmeier & Gasiewski, 2001). The complete functional operation (flightlines and mapping specifications) of PSR is given in Bindlish et al. (2005). PSR in SMEX02 used 10 frequencies (6 Ghz, 6.5 Ghz, 6.92 Ghz, 7.32 Ghz, 10.64 Ghz, 10.69 Ghz, 10.70 Ghz, 10.75 Ghz, and Thermal) for passive microwave remote sensing. Bindlish et al. (2005) closely examined the effects of RFI (Radio Frequency Interference) and reported that the 7.32 GHz and 10.7 GHz bands were far superior to the other frequencies. So the soil moisture fields of SMEX02 regions were created using these two C band channels (7.32 GHz and 10.7 GHz).



Fig. III-1. Location of SMEX02 experiment and IOWA regional study area (Bindlish et al. 2005).

Ten days of PSR based soil moisture estimates (resolution: 800 m X 800 m, size: 144 X 70 pixels) over the regional area during SMEX02 is illustrated in Fig. III-2. Bindlish et al. (2005) concluded that despite of peak crop conditions (biomass  $\sim 8 \text{ kg/m}^2$ ) encountered during the SMEX02 experiment, good results were obtained using the full soil moisture retrieval algorithm. As illustrated in Fig. III-2 there are some null values at

the bottom portion of the soil moisture fields. For this study the null values were dropped from the study region by trimming all the 10 soil moisture fields resulting in a net area of 125 X 70 pixels.

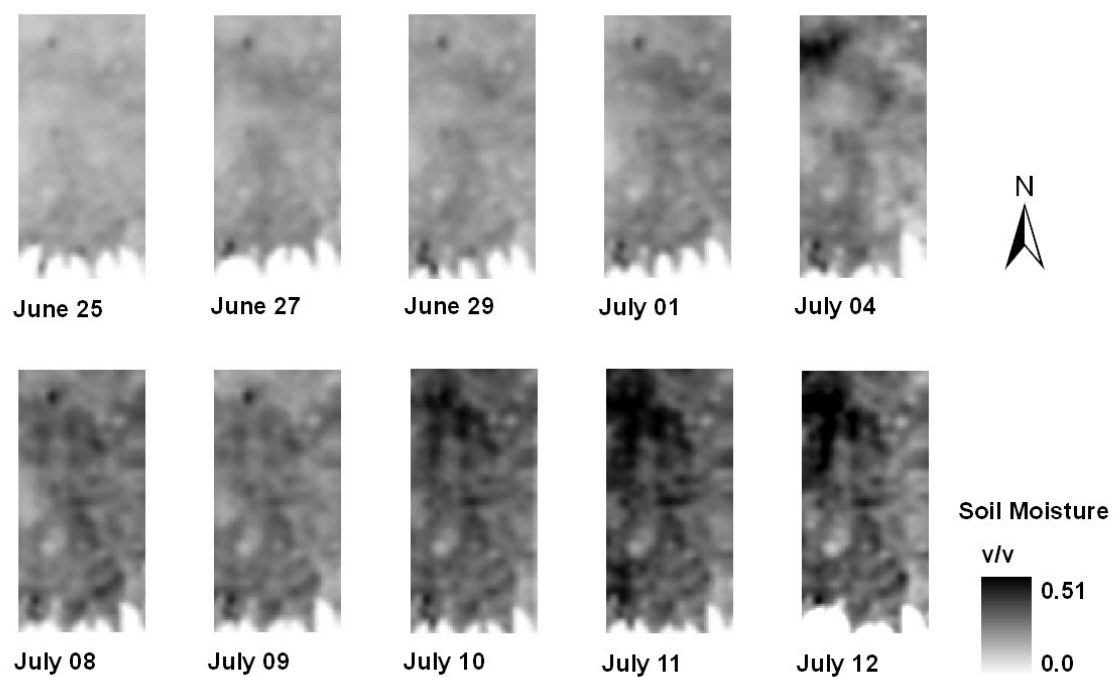


Fig. III-2. PSR (C-band single channel) based soil moisture estimates over the regional area during SMEX02.

### *Multiresolution Analysis of PSR Estimated Soil Moisture Fields*

In remote sensing context, spatial scale (resolution) is defined as the size of the smallest distinguishable part (pixel) of a spatial dataset (Lam and Quattrochi, 1992).

Spatial dataset at different scales may carry different information. Each level of spatial scales has its own unique properties that are not the simple summation of the disaggregated part (Golley, 1989). Wavelet analysis, a relatively new tool in geophysics (Kumar and Foufoula-Georgiou, 1997) has the capability to decompose the 2D-spatial dataset into average and detail components at various scales. The spatial dataset (in this study: PSR-based soil moisture field) is decomposed into average and detail components corresponding to the frequencies, and the location of those components in the space domain is also registered. The wavelet coefficient  $D$  derived from the decomposition corresponds to a wavelet function  $\psi$  of scale  $m$  and position  $n, k$  of the 2D-spatial dataset. The decomposition of the soil moisture field into wavelet and scaling function coefficient is called multiresolution analysis (Mallat, 1989). In this study a discrete wavelet transform (DWT) was used to decompose the PSR based soil moisture fields (of SMEX02) into an equally large set of scaling and wavelet coefficients. A brief description of DWT is as follows.

For a square-integrable function  $f(x)$ , the integrable wavelet transform is defined as

$$Wf(\lambda, u) = \int_{-\infty}^{\infty} f(x)\psi_{\lambda}(x-u)dx \quad \text{[III-1]}$$

where,  $u$  is the location parameter and  $\lambda$  is a dilating parameter. The function  $\psi(x)$  is called a wavelet function and the corresponding wavelet family is given by  $\sqrt{\lambda}\psi(\lambda(x-u))$ . Substituting  $x$  and  $u$  in the wavelet transform Eq. [III-1] to be vectors  $\mathbf{x} = (x_1, x_2)$  and  $\mathbf{u} = (u_1, u_2)$  respectively, a two dimensional wavelet transform is obtained.



In this study the Haar wavelet (Haar, 1910) is used to conserve the amount of information within multiresolution analysis. Haar wavelet was preferred over other wavelets because of its ability to detect rapid change during data decomposition (Mahrt, 1991). Haar wavelet  $\psi(t)$  and scaling  $\phi(t)$  function is the simplest of all orthogonal (orthonormal) wavelets (Kumar and Foufoula-Georgiou, 1997) and is given as

$$\psi(x) = \begin{cases} 1 & 0 \leq x < \frac{1}{2} \\ -1 & \frac{1}{2} \leq x < 1 \\ 0 & \text{otherwise} \end{cases} \quad \text{[III-2]}$$

$$\phi(x) = \begin{cases} 1 & 0 \leq x < 1 \\ 0 & \text{otherwise} \end{cases} \quad \text{[III-3]}$$

The orthonormal Haar wavelet family constitutes an orthonormal basis for the space  $L^2(\mathbf{R})$  which is a collection of square-integrable functions (finite energy). The square-integrable functions can be represented by a linear combination of the wavelets  $\psi_{m,n}(x)$ , i.e.

$$f(x) = \sum_{m=-\infty}^{\infty} \sum_{n=-\infty}^{\infty} D_{m,n} \psi_{m,n}(x) \quad \text{[III-4]}$$

where  $\psi_{m,n}(x)$ , the Haar wavelet family at discrete resolution level and discrete location, can be represented as

$$\psi_{m,n}(x) = \frac{1}{\sqrt{2^m}} \psi(2^{-m}(x - n2^m)) \quad \text{[III-5]}$$

where  $2^{-m}$  is the dilation parameter  $\lambda$  of Eq. [III-1] and  $n2^m$  is the location parameter  $u$  of Eq. [III-1].

The coefficient in Eq. [III-4] can be defined as

$$D_{m,n} = \int f(x)\psi_{m,n}(x)dx \quad [\text{III-6}]$$

A multiresolution analysis is a method of projecting the original signal on to coarse and coarser resolution. In practice, the multiresolution analysis is conducted over a finite level of scales  $m = 0, 1, \dots, M$ . The multiresolution analysis results in a series of approximate signals at scale  $M$  (average fields of coarsest resolution), and detail signals (detail components) at all other levels of decomposition. The additional advantage using Haar wavelet and scaling function within the multiresolution analysis is that the product at each scale level  $m$  is an aggregation of original data. With the Haar wavelet and scaling function the aggregated dataset for each scale level  $m$  would be the same as when the region observed from the same type of sensor but at a resolution equal to scale level  $m$ . Therefore, Haar wavelet is suitable to quantify the loss of information (detail components) within the dataset while decomposing a particular resolution. For two dimensional cases, based on work of Mallat (1989), the multiresolution analysis is given by

$$I_{m-1}f(x, y) = I_m f(x, y) + D_m^h f(x, y) + D_m^d f(x, y) + D_m^v f(x, y) \quad [\text{III-7}]$$

For detail multiresolution derivation, we refer the reader to Kumar and Foufoula-Georgiou (1997). The approximation of the function  $f(x, y)$  at the resolution  $m$  is characterized as inner product

$$I_m f = (f, \eta_{mnk}) \quad [\text{III-8}]$$

where  $n$  and  $k$  are location parameters. The detail components (horizontal, diagonal and vertical) of the function  $f(x, y)$  are defined as inner products

$$D_m^h f = (f, \beta^h_{mnk}) \quad [\text{III-9}]$$

$$D_m^d f = (f, \beta^d_{mnk}) \quad [\text{III-10}]$$

$$D_m^v f = (f, \beta^v_{mnk}) \quad [\text{III-11}]$$

The scaling function  $\eta$  (2-dimensional) and wavelet functions  $\beta^h$ ,  $\beta^d$  and  $\beta^v$  are created from Haar wavelet function  $\psi(x)$  Eq. [III-2] and Haar scaling function  $\varphi(x)$  Eq. [III-3], and are defined as

$$\eta(x,y) = \varphi(x) \varphi(y) \quad [\text{III-12}]$$

$$\beta^h(x,y) = \psi(x) \varphi(y) \quad [\text{III-13}]$$

$$\beta^d(x,y) = \psi(x) \psi(y) \quad [\text{III-14}]$$

$$\beta^v(x,y) = \psi(y) \varphi(x) \quad [\text{III-15}]$$

An illustration of applying the above algorithm of multiresolution analysis, the PSR based soil moisture field of July 10<sup>th</sup> 2002 (SMEX02) at the original resolution (800 m X 800 m) (Fig. III-3a (level  $m = 1$ )) decomposed into four fields of resolution 1600 m X 1600 m as illustrated in Fig. III-3b. This include one average field  $A_1$  (top left quadrant) corresponding to the scale function  $\eta$  and three fluctuation fields  $D_1^h$  (horizontal component: top right quadrant),  $D_1^d$  (diagonal component: bottom right quadrant), and  $D_1^v$  (vertical component: bottom left quadrant) corresponding to wavelets  $\beta^h(x,y)$ ,  $\beta^d(x,y)$ , and  $\beta^v(x,y)$  respectively. Similarly the average field  $A_1$  presented in Fig. III3b could be decomposed further (level  $m = 2$ ) into four fields ( $A_2$ ,  $D_2^h$ ,  $D_2^d$ , and  $D_2^v$ ) of resolution 3100 m X 3100 m. In this study 10 PSR based soil moisture fields for SMEX02 were decomposed till level  $m = 5$  (resolution: 22500 X 22500 m) for

multiresolution analysis. At each level of decomposition, the average field ( $A$ ) becomes more homogenous and the anisotropy is captured in the fluctuation components ( $D$ ). Kumar and Foufoula-Georgiou (1993a) demonstrated that the wavelet decomposition aggregate a non-stationary image into average fields ( $A$ ) which are non-stationary and fluctuation fields ( $D$ ) which are stationary. The stationary fields, which are considered as fluctuation of the process, could be used to test the presence of self-similarity (simple scaling).

The horizontal, diagonal and vertical wavelet coefficients measure the intensity of the local variation within the pixel of the soil moisture field when decomposing for a particular scale. The value of the coefficient is zero when no variation (local signal is constant) is observed within the aggregated pixel for the scale under consideration. The value of the coefficient is large when the magnitude of the wavelet is close to the scale of heterogeneity in the soil moisture field. Thus, the variance of the wavelet coefficients gives information about subpixel variability for the spatial scales in the remote sensing data (Percival, 1995). The wavelet variance is defined as

$$\sigma^2_{y,m} = \frac{1}{N} \sum D^2_{m,nk} \quad \text{[III-16]}$$

where  $\sigma^2_{y,m}$  is the wavelet variance of the spatial dataset  $y$  at scale  $m$ .  $D_{m,nk}$  are the wavelet coefficients in a particular direction at position  $nk$  and scale  $m$ .

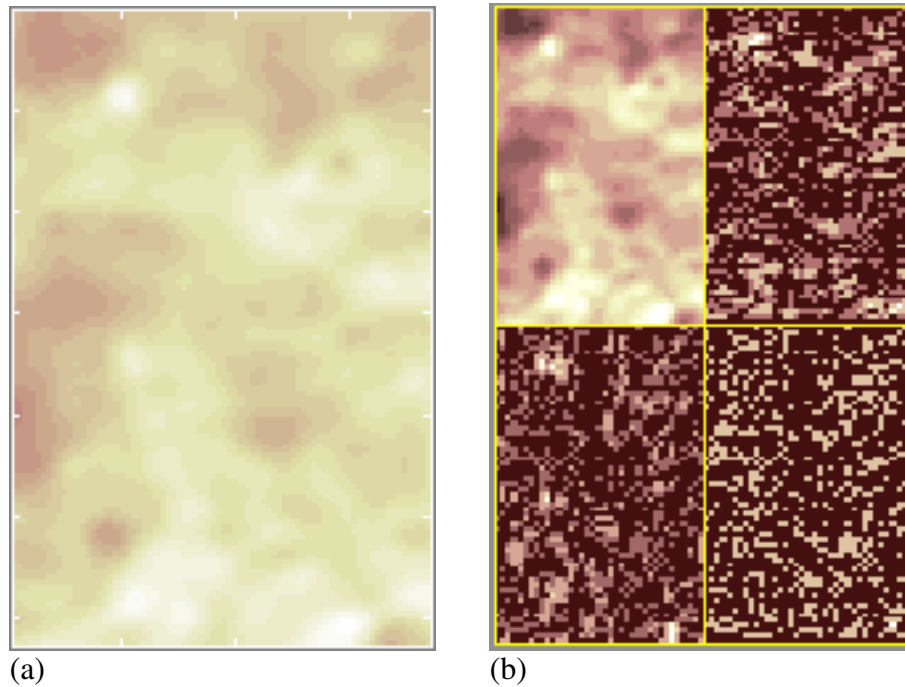


Fig. III-3. Haar wavelet decomposition of a PSR based soil moisture field. (a) Representation of original soil moisture field on June 25<sup>th</sup> 2005 of resolution 800 m X 800 m. (b) Average field  $A_I$  (top left quadrant) and three fluctuation fields  $D_I^h$  (horizontal component: top right quadrant),  $D_I^d$  (diagonal component: bottom right quadrant), and  $D_I^v$  (vertical component: bottom left quadrant) of resolution 1600 m X 1600 m.

### ***Simple Scaling and Multiscaling***

Following (Gupta and Waymire, 1990), let  $[Z(x)]$  represent an arbitrary stochastic soil moisture field of a spatial dataset indexed by vector  $x \in R^d$ , where  $R^d$  is  $d$  dimensional space. Then  $[Z(x)]$  is statistically self-similar if for any arbitrary set of points,  $x_1, x_2, x_3, \dots, x_n$ , the equality holds in the joint probability distribution of  $[Z(x)]$ :

$$P[ Z(\alpha x_1) < z_1, \dots, Z(\alpha x_n) < z_n ] = P[\alpha^{h\theta} Z(x_1) < z_1, \dots, \alpha^{h\theta} Z(x_n) < z_n] \quad \text{[III-17]}$$

where  $\alpha$  is the scale ratio and  $h\theta$  is a real scaling exponent. For simple scaling there is only one scaling exponent  $h\theta$  and the process is said to be “fractal” or “mono-fractal”.

The expected moment of stochastic field can then be related to this single value as a function of scale:

$$E[ Z^p(\alpha) ] = \alpha^{ph\theta} E[ Z^p(l) ] \quad \text{[III-18]}$$

where  $p$  is the order of the moment, taking log of both side of Eq. [III-18],

$$\log m_p(\alpha) = s(p) \log \alpha + \log m_p(l) \quad \text{[III-19]}$$

where  $m_p(\alpha) = E[ Z^p(\alpha) ]$  and  $s(p) = ph\theta$ . For simple scaling process the log-log linearity in  $\log m_p(\alpha)$  versus  $\log \alpha$  for each  $p$  and, linearity of the slope  $s(p)$  change for each  $p$  must be satisfied. If  $s(p)$  is a nonlinear function of  $p$  the process has multiscaling properties. In this study, for the soil moisture field the scale factor  $\alpha = A_i / A_0$ , where  $A_i$  is any pixel area obtained from aggregation from the original (remote sensor) pixel area and  $A_0$  is the coarsest pixel area after aggregation (multiresolution analysis).

One more type of scaling typically found in soil moisture fields is the power law scaling of variance of soil moisture contents (Hu et al., 1997)

$$Var_L = (\alpha)^h Var_a \quad \text{[III-20]}$$

where  $Var_L$  is the variance at the aggregated level,  $Var_a$  is the variance in the original soil moisture field,  $\alpha$  is the scale-factor defined as before and  $h$  is the slope. The exponent of the power law is found to be an index for the spatial correlation structure of the soil moisture field. An exponent of -1 refers to a spatially independent identical distribution process, while an exponent of 0 indicates a completely spatially correlated structure.

## Results and Discussion

The 10 days of PSR based soil moisture fields during SMEX02 (Fig. III-2) were decomposed (multiresolution analysis) till level 5. The decomposition resulted in 5 coarser resolution fields (1600 m X 1600 m, 3100 m X 3100 m, 6100 m X 6100 m, 12100 m X 12100 m, and 22500 m X 22500 m) of average soil moisture from the base resolution of 800 m X 800 m. The decomposition also resulted in 3 fluctuation fields (horizontal, diagonal, and vertical) for each level of decomposition at 5 coarser resolutions. Five scale factors ( $\log(\alpha) = \log(A_i / A_0)$ : -5.3, -3.9, -2.6, -1.2, 0) corresponding to decomposed resolutions were calculated with  $A_0$  as the area of coarsest resolution (22500 m X 22500 m).

### *Analysis of Power Law Scaling*

The mean of soil moisture fields at various resolutions is plotted against log of scale factors in Fig. III-4. Three distinct groups are clearly visible in the plot (Fig.III-4); the upper most group is of the wet fields (July 10<sup>th</sup>, July 11<sup>th</sup>, and July 12<sup>th</sup>), the intermediate group is the partially dry fields (July 1<sup>st</sup>, July 4<sup>th</sup>, July 8<sup>th</sup>, and July 9<sup>th</sup>) and the lower most group is of the dry fields (June 25<sup>th</sup>, June 27<sup>th</sup> and June 29<sup>th</sup>) during the SMEX02.

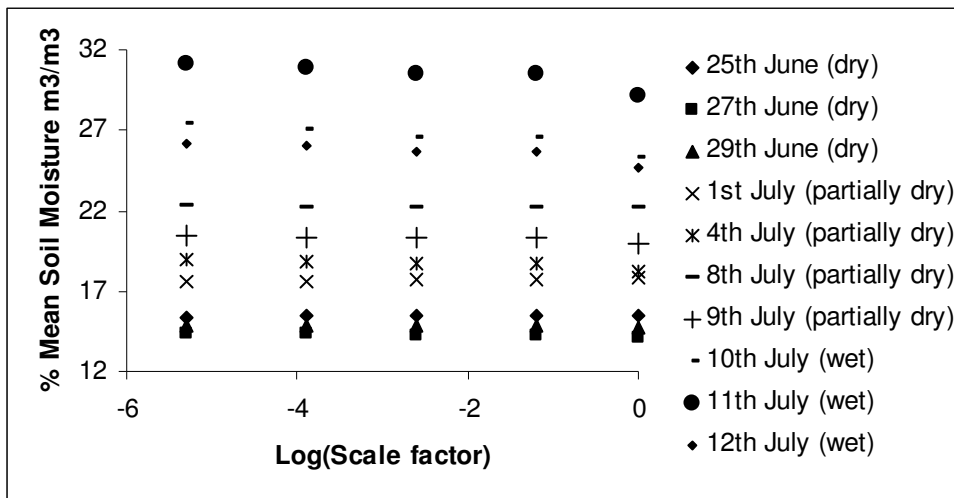


Fig. III-4. Mean of soil moisture against log of scale-factors.

The variance for average soil moisture fields is plotted against scale factors on a log-log plot in Fig. III-5. Like Fig. III-4, similar three groups are clearly visible in the Fig. III-5, with one exception of July 4<sup>th</sup>, 2002 which shows high soil moisture variance due to scattered rainfall. The discussion of Sellers et al. (1995) about high spatial heterogeneity introduced by rainfall and removed through dry-down dynamics is also found applicable here at all scale factors. Linearity in the log-log dependency of the variance on scale factors Eq. [III-20] can be observed in Fig. III-5. In this study, linearity is observed up to scale factor of -2.6 (6100 m<sup>2</sup>). Rodriguez-Iturbe et al. (1995) reported linear scaling up to 1000 m<sup>2</sup> for the Washita '92 soil moisture data. Hu et al. (1997) found the linearity up to 32000 m<sup>2</sup> for the same dataset (Washita '92) using a different aggregation scheme. Oldak et al. (2002) demonstrated that for ESTAR dataset during SGP97 the linearity was observed up to 7800 m<sup>2</sup>. Another apparent characteristic is the near linearity of variance against scale factors for the wet fields (Fig. III-5). The near



zero slope for the wet fields indicate almost similar variance for all the scale factors (a strong spatial correlation). However, higher soil moisture variability at all scale factors is observed in wet fields due to variability present in precipitation pattern (Kumar and Foufoula-Georgiou, 1993a) over the study area. The variability at any given scale factor becomes smaller as the drydown progresses (Fig. III-5). In Fig. III-5 a very low variance at scale factor 0 (22500 m X 22500 m) for the driest field (June 29<sup>th</sup>) indicates an almost uniform soil moisture field. A least square fit slope of approximately -0.23 is observed for all dry fields, which is consistent with the slope reported by (Hu et al., 1997). As the slope of the log (variance) across scales remains almost constant for the dry fields, the temporal decrease in variability were mostly related to the decrease in intercepts suggesting a proportional drydown.

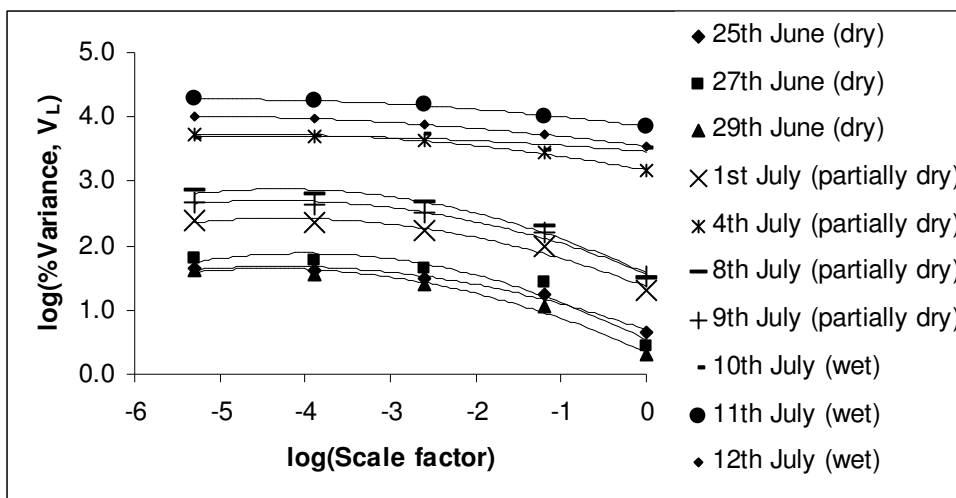
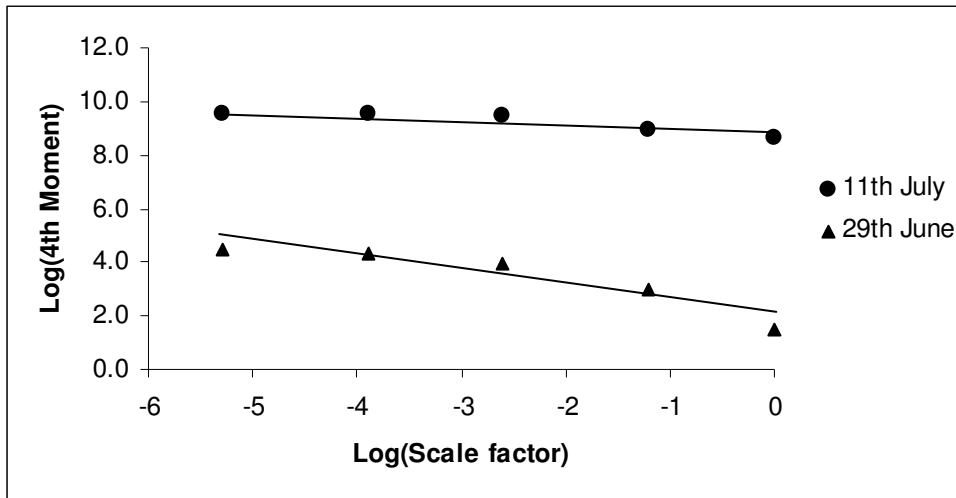


Fig. III-5. Dependencies of the variance of soil moisture against scale –factors in a log-log plot.

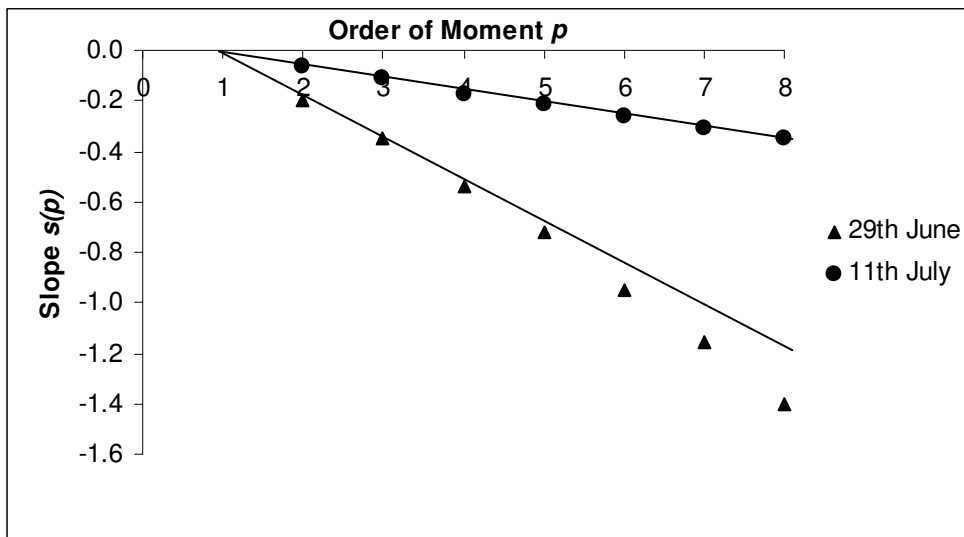
### ***Scaling Analysis of Soil Moisture Fields***

Scaling analysis was conducted for all the soil moisture fields of SMEX02. Eight moments were calculated for each scale factor of the soil moisture fields. Figure III-6a illustrates log-log dependency of 4<sup>th</sup> moment of June 29<sup>th</sup> (dry field) and July 11<sup>th</sup> 2002 (wet field) plotted against scale factors. Similarly 2<sup>nd</sup> to 8<sup>th</sup> moments were plotted against scale factors in a log-log plot for all the soil moisture fields (Fig. III-6b). The slope in Eq. [III-19] was estimated by linear regression for moment order  $p$  (2<sup>nd</sup> to 8<sup>th</sup> moment) with high  $R^2$  (coefficient of determination). Linearity is observed up to scale factor of -2.6 (6100 m<sup>2</sup>) for all sampling days of SMEX02, as for variance (results not shown here). It was also observed that the slope become smaller for higher order moments. For illustration, slopes of June 29<sup>th</sup> (dry field) and July 11<sup>th</sup> (wet field) are plotted against moment order  $p$  in Fig. III-6b. To exhibit simple scaling process, the rate of change of the slope with respect to moment order is equal to the slope at the 1<sup>st</sup> moment (Gupta and Waymire, 1990). The expected value of first moment about mean is 0 and consequently the slope is always 0 for the first moment. A straight line is plotted based on slope of 1<sup>st</sup> and 2<sup>nd</sup> orders of moments in Fig. III-6b. From Fig. III-6b for June 29<sup>th</sup> (dry field) a non-constant rate of change of slope (non-linear, downward open concave function) with respect to moment order indicates that soil moisture does not obey a simple scaling law, therefore a multiscaling process. Multiscaling property was observed for all the dry fields of SMEX02. Gupta and Waymire (1990) found slope in the range of -5 to 0 for rainfall analysis, which is much higher in absolute value than the slope we found in the present study. On the contrary, Wood (1994) found an upward concave function

relationship between the slope and the order of moment for the scaling properties of soil moisture fields simulated from the coupled water-energy model. Hu et al. (1998) and Oldak et al., (2002) demonstrated similar multiscaling for the dry fields of Washita '92 and SGP97 experiments, respectively. Another important finding of scaling characteristics of this study was simple scaling for all the wet fields during SMEX02. The scaling exponent during drydown suggest a transition from simple scaling (in wet fields) to multiscaling (in dry fields). As illustrated in Fig. III-6b, wet field of SMEX02 on July 11<sup>th</sup> 2002 obey simple scaling law when slope measured at 1<sup>st</sup> moment for all the values of slopes with respect to the order of moments  $p$ . Therefore, the study support the conclusion of Dubayah et al. (1997), Hu et al. (1998) and Oldak et al. (2002) that the multiscaling (mutifractal) scaling is an appropriate statistical model for soil moisture spatial distribution during the drydown.



(a)



(b)

Fig. III-6. (a) Linear fit for moment of order four versus scale-factors on a log-log plot for average soil moisture fields of June 29<sup>th</sup> (slope  $s(p) = -0.54$ , and  $R^2 = 0.85$ ) and July 11<sup>th</sup> 2002 (slope  $s(p) = -0.17$ , and  $R^2 = 0.9$ ). (b) Deviation and conformance to simple scaling in the change of slopes with respect to order of moments for soil moisture fields of June 29<sup>th</sup> and July 11<sup>th</sup> 2002 (SMEX02), respectively.

### Wavelet Variance

The fluctuation fields (horizontal, diagonal and vertical wavelet coefficients) measure the intensity of the local variation of soil moisture within the scale factor (resolution). Wavelet variance Eq. [III-16] for horizontal, diagonal and vertical wavelet coefficients were calculated for each level of scale factor. Fig. III-7 shows the wavelet variance of horizontal component against the log of scale factor for June 29<sup>th</sup> (dry field) and July 11<sup>th</sup> (wet field) of SMEX02. Fig. III-7 illustrates an interesting feature of subpixel variability present in a dry versus a wet field at various scale-factors. At a smaller scale-factor (-5.3) the soil moisture variability is almost similar for both scenarios, whereas for higher scale-factors (-3.9, -2.6, -1.2, 0) the difference in soil moisture variability between dry and wet fields increases with increasing scale-factor.

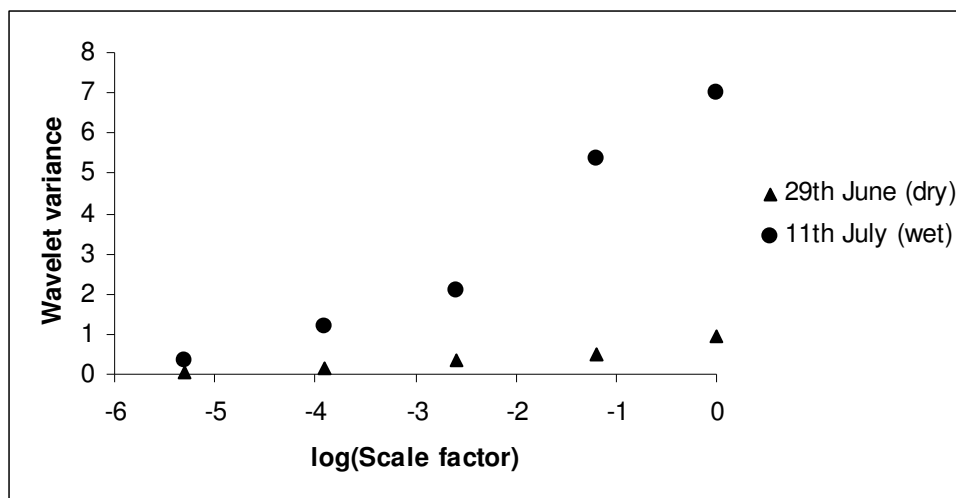


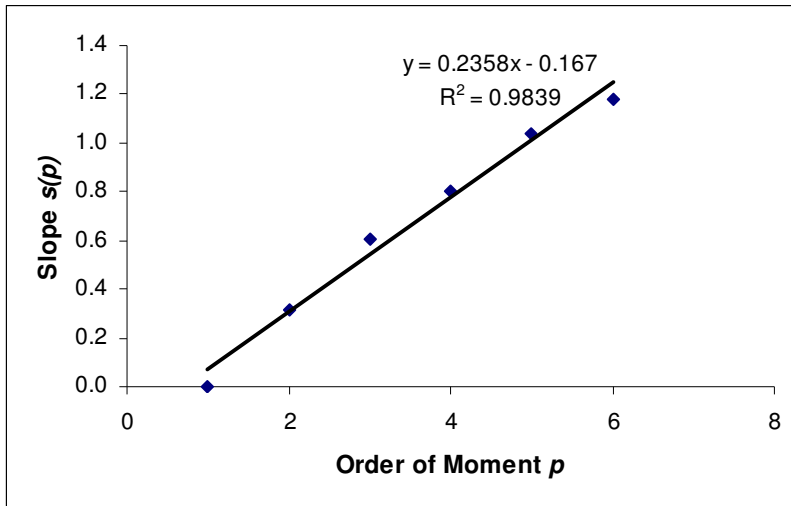
Fig. III-7. Wavelet variance versus scale factor in log-log plot for fluctuation fields (horizontal direction) on June 29<sup>th</sup> and July 11<sup>th</sup> 2002 (SMEX02).

### ***Study of Self Similarity***

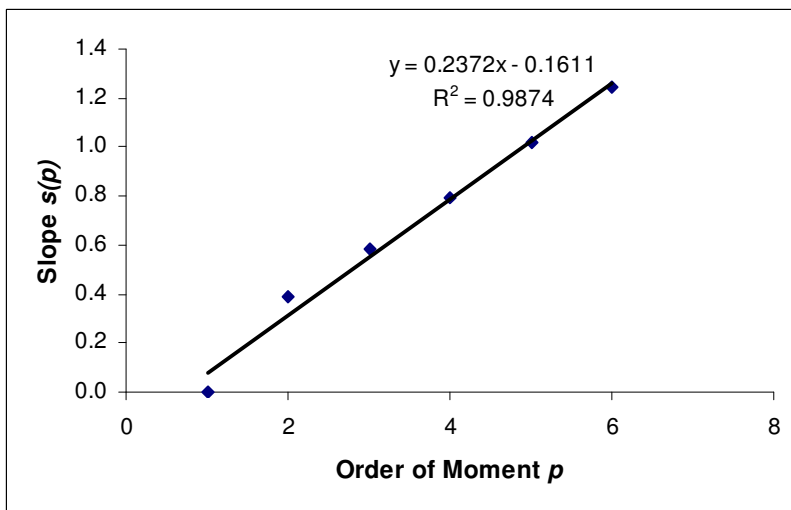
To examine self-similar nature of soil moisture fields of SMEX02, the first six moments of wavelet coefficients of fluctuation fields (horizontal, diagonal and vertical components) were calculated for each level of decomposition (multiresolution analysis). Table III-1 presents the slope in Eq. [III-19] and  $R^2$  for the order of moment versus scale factor in a log-log plot for all the fluctuation fields of June 29<sup>th</sup> (dry field) and July 11<sup>th</sup> (wet field) of SMEX02. It is apparent from Table III-1 that as the order of moment increases, the value of slope increases and  $R^2$  decreases. The linearity of regression (high  $R^2$ ) suggests presence of self similarity. Fig. III-8a-c and Fig. III-9a-c illustrate the rate of change of slope with respect to moment order  $p$  for three fluctuation components of June 29<sup>th</sup> (dry field) and July 11<sup>th</sup> (wet field) of SMEX02, respectively. Once again, linear regression techniques were used to determine the slope in Fig. III-8a-c and Fig. III-9a-c, and the values are shown in the figures. A constant rate of change from the 1<sup>st</sup> order moment indicates simple scaling in all the three directions.

Table III-1. Results of regression: slope  $s(p)$ , coefficient of determination  $R^2$  for order of moment versus scale-factors in horizontal, vertical and diagonal directions stationary fluctuation components) for PSR based soil moisture estimates of SMEX02.

SMEX02	Horizontal		Diagonal		Vertical	
June 29th 2002						
Order of Moment						
$p$	Slope $s(p)$	$R^2$	Slope $s(p)$	$R^2$	Slope $s(p)$	$R^2$
1	0	NA	0	NA	0	NA
2	0.318	0.99	0.387	0.98	0.355	0.91
3	0.609	0.96	0.580	0.95	0.549	0.91
4	0.804	0.92	0.792	0.94	0.800	0.90
5	1.040	0.86	1.016	0.94	0.943	0.87
6	1.179	0.81	1.241	0.91	1.161	0.85
July 11th 2002						
Order of Moment						
$p$						
1	0	NA	0	NA	0	NA
2	0.410	0.96	0.591	0.93	0.288	0.92
3	0.650	0.93	1.192	0.93	0.560	0.92
4	0.928	0.89	1.599	0.93	0.831	0.86
5	1.189	0.86	1.997	0.93	0.998	0.82
6	1.339	0.83	2.379	0.92	1.163	0.79



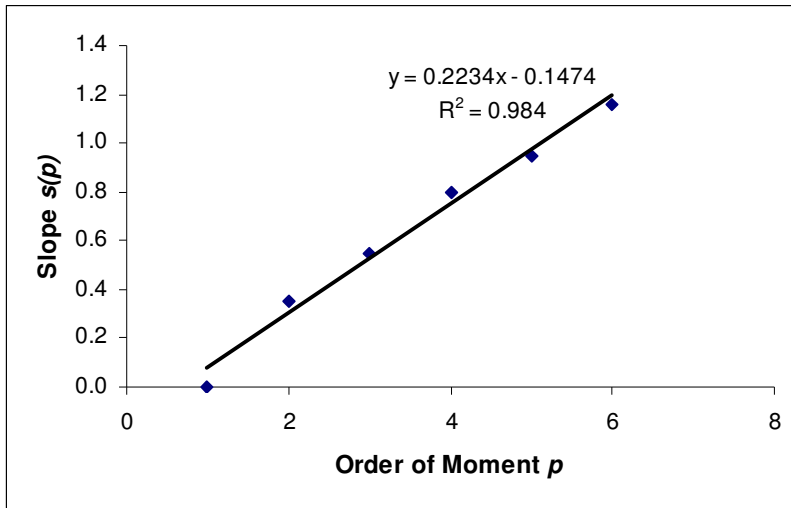
(a)



(b)

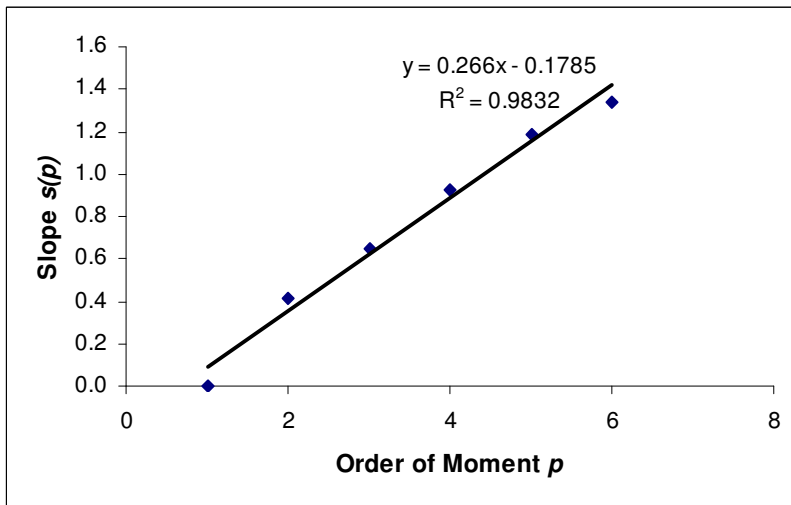
Fig. III-8. Slope  $s(p)$  versus order of moment  $p$  plots for fluctuations fields on June 29<sup>th</sup> 2005 (SMEX02): (a) horizontal, (b) diagonal and (c) vertical directions.





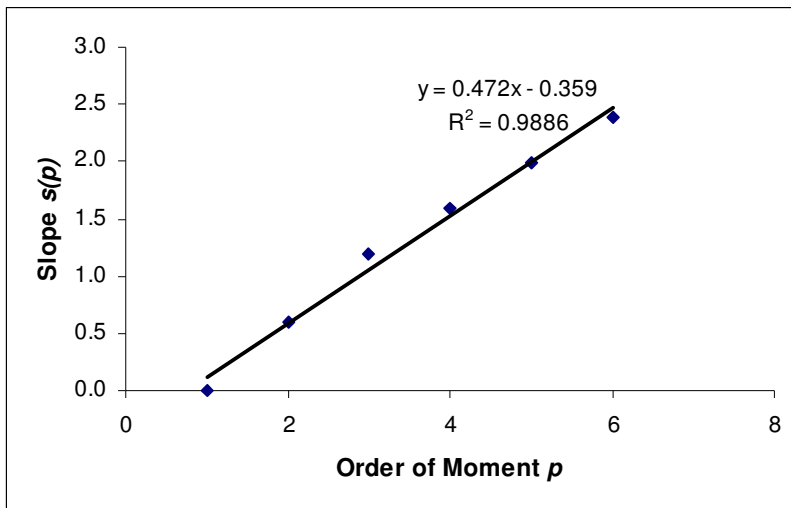
(c)

Fig. III-8. Continued.

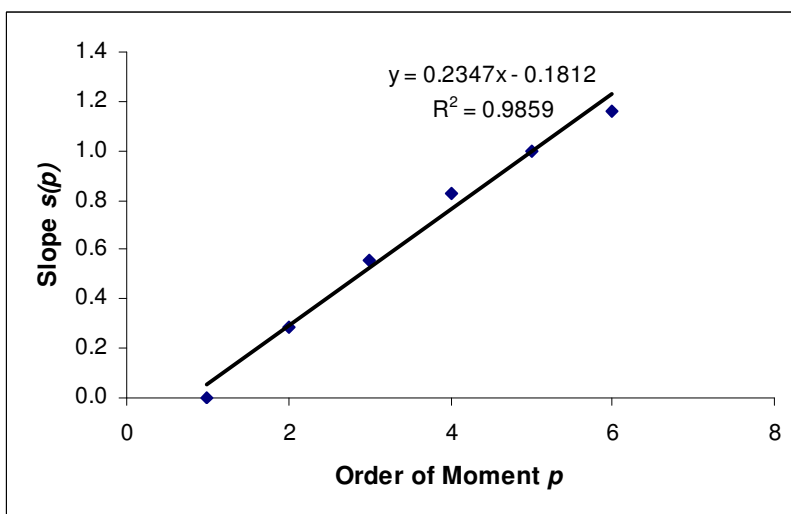


(a)

Fig. III-9. Slope  $s(p)$  versus order of moment  $p$  plots for fluctuations fields on July 11<sup>th</sup> 2005 (SMEX02): (a) horizontal, (b) diagonal and (c) vertical directions.



(b)



(c)

Fig. III-9. Continued.

The regression resulted in slope ranging from 0.22 to 0.266 except for diagonal component of July 11<sup>th</sup> 2002 (wet field) of SMEX02, which is 0.472. A range of slopes (0.22 to 0.266) for fluctuation fields in horizontal and vertical directions between a dry

(June 29<sup>th</sup>) and wet field (11<sup>th</sup> July) indicates minimal change in self-similarity pattern during drydown from wet field to dry field. This is an important observation in the sense that, although wet fields show higher soil moisture variability (higher wavelet variance) at any given resolution, they showed similar horizontal and vertical fluctuation fields as the dry fields for all the scale-factors. The difference of slope in diagonal direction for the wet field suggests change in self similarity pattern along the diagonal direction. It is also interesting to note that the positive slope is observed which is opposite to what found by Hu et al. (1998) in their study of fluctuation fields in Little Washita watershed using the ESTAR microwave data collected during Washita '92 and, Brunsell and Gillies (2003) examination of self similarity present in AVHRR data of July 2<sup>nd</sup> 1997 in the SGP97 region. The positive slope is due to increase in subpixel variability with increasing scale factors.

### **Conclusion**

We have examined the spatial structure of PSR based soil moisture fields of SMEX02 using Haar wavelet multiresolution analysis. SMEX02 regional area was nearly 95% of row crop agriculture (corn and soybean). The multiresolution study was conducted on 5 distinct scale-factors (resolutions). Our finding of scaling properties for the soil moisture fields of SMEX02 also confirms the previous finding that soil moisture follows power law scaling with increasing scale-factors. The spatial structure of soil moisture exhibited linearity in the log-log dependency of the variance versus scale-

factor, up to a scale factor of  $-2.6$  ( $6100 \text{ m}^2$ ) irrespective of wet or dry fields. The study also support increase in variability with precipitation for all the scale-factors and also show remarkable increase in sub-pixel variability with increasing scale-factors for all wet days. It is also shown that once a dependency on scale factor is established at the beginning of drying period, its shape is maintained during the drydown. Slope of the dependencies almost remains the same where as the intercept decrease as the drying progresses. The scaling exponent during drydown suggest a transition from simple scaling (in wet fields) to multiscaling (in dry fields). The fluctuation fields (horizontal, diagonal and vertical wavelet coefficients) measure the intensity of the local variation of soil moisture within the scale factor (resolution). These fluctuation fields indicated simple scaling, with similar simple scaling properties observed in horizontal and vertical directions for dry and wet days, whereas difference in self-similarity property was detected in diagonal direction of wet and dry fields. The results of this work (i.e. the statistical variability of soil moisture with changing spatial resolution in an area of row crop agriculture) contribute to basic understanding how to assimilate remotely sensed data of high agricultural landscape (corn and soybean) into ecological and climatological modeling.

## CHAPTER IV

### GENERAL CONCLUSIONS

This study deals with modeling of root zone soil moisture and scaling of surface soil moisture. Two studies were conducted from two different hydrology experiments (SGP97 and SMEX02) and highlighted the importance of spatio-temporal variability present in surface and root zone soil moisture. The study also demonstrated the modeling and scaling challenges introduced by soil moisture distribution present across space and time, and most importantly, the spatial distribution of soil, vegetation and precipitation which controls the distribution of soil moisture in space. Better methods for defining the accuracy in precipitation, and spatial properties for soil and vegetation as they affect soil moisture are key challenges for the spatially-distributed SMAT model. Sequential data assimilation (EnKF) formulated for SMAT is flexible and can be tested for deeper soil profile. The SMAT model can readily trade off estimation accuracy and computational demands by simply adjusting the number of ensemble members. The significance of results from second study (wavelet based multiresolution analysis) is that it provides a possible direction for development of downscaling algorithm that can capture the spatio-temporal scaling properties of soil moisture. Wavelet based multiresolution analysis can make available data from passive microwave remote sensing platforms to model root zone soil moisture at various resolutions. Further research and investigation is essential in variety of hydroclimatic conditions to improve the performance of scaling and modeling scheme developed/evaluated in this work. This study leads to an ultimate goal

of establishing an operational platform for assessing surface and root zone soil moisture at various spatial resolutions from space-borne passive microwave remote sensors.

## REFERENCES

- Allen, P.B., and J.W. Naney. 1991. Hydrology of Little Washita river watershed, Oklahoma: Data and Analyses. US Department of Agriculture, Agriculture Research Service, USDA Technical Report ARS-90, 74.
- Bindlish, R., W.P. Kustas, A.N. French, G.R. Diak, and J.R. Mecikalski. 2001 Influence of near-surface soil moisture on regional scale heat fluxes: Model results using microwave remote sensing data from SGP97, *IEEE Trans. Geosci. Remote Sens.* 39:1719–1728.
- Bindlish, R., T.J. Jackson, A.J. Gasiewski, M. Klein, and E.G. Njoku. 2005. Soil moisture mapping and AMSR-E validation using the PSR in SMEX02. *Remote Sens. of Environ.* In press.
- Brunsell, N.A., and R.R. Gillies. 2003. Determination of scaling characteristics of AVHRR data with wavelets: application of SGP97. *Int. J. Remote Sens.* 24:2945-2957.
- Camillo, P., and T.J. Schugge. 1983. Estimating soil moisture storage in the root zone from surface measurements. *Soil Sci.* 135(4):245-264.
- Carsel, R.F., and R.S. Parrish. 1988. Developing joint probability distributions of soil water retention characteristics. *Water Resour. Res.* 24:755-769.
- Chen, F., K. Mitchell, J. Schaake, Y. Xue, H.L. Pan, V. Koren, Q.Y. Duan, M. Ek, and A. Betts. 1996. Modeling of land-surface evaporation by four schemes and comparison with FIFE observations. *J. Geophys. Res.* 101:7251–7268.
- Cosh, M.H., and W. Brutsaert. 1999. Aspect of soil moisture variability in the Washita '92 study region. *J. Geophys. Res.* 104(19):751-757.
- Crosson, W.L., C.A. Laymon, R. Inguva, and M.P. Schamschula. 2002. Assimilating remote sensed data in a surface flux-soil moisture model. *Hydrol. Process.* 16:1665-1662.
- Crow, W.T., and E.F. Wood. 2003. The assimilation of remotely sensed soil brightness temperature imagery into a land surface model using ensemble Kalman filtering: A case study based on ESTAR measurements during SGP97. *Adv. Water Resour. Res.* 26:137-149.
- Crow, W.T., R. Dongryeol, and J.S. Famiglietti. 2005. Upscaling of field-scale soil moisture measurement using distributed land surface modeling. *Adv. Water Resour.*

28:1-14.

Dai, Y., X. Zeng, R.E. Dickinson, I. Baker, G.B. Bonan, M.G. Bosilovich, A.S. Denning, P.A. Dirmeyer, P.R. Houser, G. Niu, K.W. Oleson, C.A. Schlosser, and Z.-L. Yang. 2003. The Common Land Model (CLM). *Bull. Am. Meteorol. Soc.* 84(4):1013-1023.

Dingman, S.L. 1994. *Physical Hydrology*. Macmillan, New York.

Dubayah, R., E.F. Wood, and D. Lavallee. 1997. Multiscaling analysis in distributed modeling and remote sensing: an application using soil moisture. In: Quatrocchi, D.A., and M. Goodchild (Eds). *Scale in Remote Sensing and GIS*. Lewis Publishers, New York, pp.93-112.

Dunne, S., and D. Entekhabi. 2005. An ensemble-based reanalysis approach to land data assimilation. *Water Resour. Res.* 41: 10.1029/2004.

Engman, E.T., and R.J. Gurney. 1991. *Remote Sensing in Hydrology*. Chapman and Hall, London, UK.

Entekhabi, D., H. Nakamura, and E.G. Njoku. 1994. Solving the inverse-problem for soil moisture and temperature profiles by sequential assimilation of multifrequency remotely sensed observations, *IEEE Trans. Geosci. Remote Sensing* 32:438-448.

Entin, J.K., A. Robock, K.Y. Vinnikov, S.E. Hollinger, S.X. Liu, and A. Namkhai. 2000. Temporal and spatial scales of observed soil moisture variations in the extratropics. *J. Geophys. Res.-Atmo.* 105:11865-11877.

Evensen, G. 2003. The ensemble Kalman filter: Theoretical formulation and practical implementation. *Ocean Dynamics* 53:343-367.

Famiglietti, J.S., J.A. Devereux, C.A. Laymon, T. Tsegaye, P.R. Houser, T.J. Jackson, S.T. Graham, and M. Rodell. 1999. Ground-based investigation of soil moisture variability within remote sensing footprints during the Southern Great Plains 1997 (SGP97) Hydrology Experiment. *Water Resour. Res.* 35(6):1839-1851.

Feddes, R.A., P.J. Kowalik, and H. Zaradny. 1978. *Simulation of Field Water Use and Crop Yield*. John Wiley and Sons, New York, NY.

Francis, C.F., J.B. Thornes, A. Romero Daiz, F. Lopez Bermudez, and G.C. Fisher. 1986. Topographic control of soil moisture, vegetation cover and land degradation in a moisture stressed Mediterranean environment. *Catena.* 13:211-225.

Georgakakos, K.P. 1996. Soil moisture theories and observations (special issue). *J.*



- Hydrol. 184:131-152.
- Golley, F.B. 1989. A proper scale: Comments of the editor. *Landscape Ecology*. 2:71-72.
- Gupta, V., and E. Waymire. 1990. Multiscaling properties of spatial rainfall and river flow distribution. *J. Geophys. Res.* 95:1999-2009.
- Haar, A. 1910. Zur theorie der orthogonalen funktionensysteme. *Math. Ann.* 69:331-371.
- Hanson, J.D., K.W. Rojas, and M.J. Schaffer. 1999. Calibrating the root zone water quality model. *Agron. J.* 91:171-177.
- Hawley, M.E., R.H. McCuen, and T.J. Jackson. 1982. Volume-accuracy relationship in soil moisture sampling. *J. Irrig. Drain. Div.* 108(IR1):1-11.
- Heathman, G.C., P.J. Starks, L.R. Ahuja, and T.J. Jackson. 2003. Assimilation of surface soil moisture to estimate profile soil water content. *J. Hydrol.* 279:1-17.
- Hellweger F.L. and D.R. Maidment. 1999. Definition and connection of hydrologic elements using geographic data. *J. Hydraulic Eng.* 4:10-8.
- Hook, W.R., and N.J. Livingston. 1996. Errors in converting time domain reflectometry measurements of propagation velocity to estimates of soil water content. *Soil Sci. Soc. Am. J.* 60:35-41.
- Houser, P.R., W.J. Shuttleworth, J.S. Famiglietti, H.V. Gupta, K.H. Syed, and D.C. Goodrich. 1998. Integration of soil moisture remote sensing and hydrologic modeling using data assimilation. *Water Resour. Res.* 34(12):3405-3420.
- Hu, Z., S. Islam, and Y. Chen. 1997. Statistical characterisation of remotely sensed soil moisture image. *Remote Sens. of Environ.* 61: 301-318.
- Hu, Z., Y. Chen, and S. Islam. 1998. Multiscaling properties of soil moisture image and decomposition of large scale and small scale features using wavelet transform. *Int. J. Remote Sens.* 19:2451-2467.
- Hupet, F., and M. Vanclooster. 2002. Intraseasonal dynamics of soil moisture variability within a small agricultural maize cropped field. *J. Hydrol.* 261(1-4):86-101.
- Jackson, T.J., and T.J. Schmugge. 1989. Passive microwave remote sensing system for soil moisture: some supporting research. *IEEE Trans. Geosci. Remote Sens.* GE-27:35-46.

- Jackson, T.J. 1993. Measuring surface soil moisture using passive microwave remote sensing. *Hydrol. Process.* 7:139–152.
- Jackson, T.J., D.M. Le Vine, C.T. Swift, T.J. Schmugge, and F.R. Schiebe. 1995. Large scale mapping of soil moisture using the ESTAR passive microwave radiometer in Washita '92. *Remote Sens. of Environ.* 53:27-37.
- Jackson, T.J., D.M. Le Vine, A.Y. Hsu, A. Oldak, P.J. Starks, C.T. Swift, J.D. Isham, and M. Hakan. 1999. Soil moisture mapping at regional scales using microwave radiometry: The Southern Great Plains hydrology experiment. *IEEE Trans. Geosci. Remote Sens.* 37:2136–2151.
- Jackson, T.J., R. Bindlish, A.J. Gasiewski, B. Stankov, M. Klein, E.G. Njoku, D. Bosch, T.L. Coleman, C. Laymon, and P.J. Starks. 2005. Polarimetric scanning radiometer C and X band microwave observations during SMEX03. *IEEE Trans. Geosci. Remote Sens.*, in press.
- Koster, R., and M. Suarez. 1996. Energy and water balance calculation in the mosaic LSM. Technical Memorandum 1046069. NASA GSFC, Greenbelt, MD.
- Koster, R.D., and P.C.D. Milly. 1997. The interplay between transpiration and runoff formulations in land surface schemes used with atmospheric models. *J. Clim.* 10:1578-1594.
- Kostov, K.G., and T.J. Jackson. 1993. Estimating profile soil moisture from surface layer measurement- A review. *SPIE* 1941:125– 136.
- Kumar, P., and E. Foufoula-Georgiou. 1993a. A multicomponent decomposition of spatial rainfall fields 1. Segregation of large- and small-scale features using wavelet transforms. *Water Resour. Res.* 29:2515-2532.
- Kumar, P., and E. Foufoula-Georgiou. 1993b. A multicomponent decomposition of spatial rainfall fields 1. Self-similarity in fluctuations. *Water Resour. Res.* 29:2533-2544.
- Kumar, P., and E. Foufoula-Georgiou. 1997. Wavelet analysis for geophysical applications. *Reviews of Geophysics.* 35:385-412.
- Kumar, P. 1999. A multiple scale state –space model for characterizing subgrid scale variability of near-surface soil moisture. *IEEE Transaction on Geosciences and Remote Sensing.* 37:182-197.
- Kustas, W.P., T.J. Jackson, A.N. French, and J.I. MacPherson. 2001. Verification of patch- and regional-scale energy balance estimates derived from microwave and

- optical remote sensing during SGP97. *J. Hydrometeorol.* 2(3):254–273.
- Lachassagne, P., R. Wyns, P. Berard, T. Bruel, L. Chery, T. Coutand, J.-F. Desprats, and P. Le Strat. 2001. Exploitation of high-yields in hard-rock aquifers; downscaling methodology combining GIS and multicriteria analysis to delineate field prospecting zones. *Ground Water* 39(4):568-581.
- Lam, N., and D.A. Quattrochi. 1992. On the issues of scale, resolution, and fractal analysis in the mapping sciences. *Prof. Geogr.* 44:88-98.
- Liang, X., E.F. Wood, and D.P. Lettenmaier. 1996. Surface soil moisture parameterization of the VIC-2L model: Evaluation and modifications. *Global Planetary Change.* 13:195-206.
- Mahrt, L. 1991. Eddy asymmetry in the shear heated boundary layer. *Journal of Atmospheric Sciences.* 48:471-492.
- Mallat, S. 1989. A theory of multiresolution signal decomposition: The wavelet representation. *IEEE Transaction of Pattern. Anal. Mech. Intel.* 11(7):674-693.
- Margulis, S.A., D. McLaughlin, D. Entekhabi, and S. Dunne. 2002. Land data assimilation and estimation of soil moisture using measurements from the Southern Great Plains 1997 Field Experiment. *Water Resour. Res.* 38(12):1299-1317.
- Mitas, L., and H. Mitasova. 1998. Distributed soil erosion simulation for effective erosion prevention. *Water Resour. Res.* 34:505-16.
- Mohanty, B.P., T.H. Skaggs, and J.S. Famiglietti. 2000a. Analysis and mapping of field-scale soil moisture variability using high-resolution, ground-based data during the Southern Great Plains 1997 (SGP97) Hydrology Experiment, *Water Resour. Res.* 36(4):1023–1031.
- Mohanty, B.P., J.S. Famiglietti, and T.H. Skaggs. 2000b. Evolution of soil moisture spatial structure in a mixed vegetation pixel during the Southern Great Plains 1997 (SGP97) Hydrology Experiment. *Water Resour. Res.* 36(12):3675–3686.
- Mohanty, B.P., and T.H. Skaggs. 2001. Spatio-temporal evolution and time-stable characteristics of soil moisture within remote sensing footprints with varying soil, slope, and vegetation. *Adv. Water Resour.* 24(9–10):1051–1067.
- Mohr, K.I., J.S. Famiglietti, A. Boone, and P.J. Starks. 2000. Modeling soil moisture and surface flux variability with an untuned land surface scheme: A case study from the Southern Great Plains 1997 Hydrology Experiment. *J. Hydrometeorol.* 1(2):154–169.

- Mualem, Y. 1976. A new model predicting the hydraulic conductivity of unsaturated porous media. *Water Resour. Res.* 12:513-522.
- Njoku, E.G., and D. Entekhabi. 1995. Passive remote sensing of soil moisture. *J. Hydrol.* 184(1):101-130.
- Novak, V. 1987. Estimation of soil-water extraction patterns by roots. *Agricultural Water Management.* 12(4):271-278.
- Nyberg, L. 1996. Spatial variability of water content in the cover catchment at Gardsjon, Sweden. *Hydrol. Process.* 10:89-103.
- Nykanen, D.K., E. Foufoula-Georgiou. 2001. Soil moisture variability and scale-dependency of nonlinear parameterizations in coupled land-atmosphere models. *Adv. Water Resour.* 24:1143-1157.
- Oldak, A., Y. Pachepsky, T.J. Jackson, and W.J. Rawls. 2002. Statistical properties of soil moisture images revisited. *J. Hydrol.* 255:12-24.
- Paniconi C., S. Kleinfeldt, J. Deckmyn, and A. Giacomelli., 1999. Integrating GIS and data visualization tools for distributed hydrologic modeling. *Trans. GIS* 3:97-118.
- Percival, D. 1995. On estimation of wavelet variance. *Biometrika.* 82:619-631.
- Peters-Lidard, C.D., F. Pan, and E.F. Wood. 2001. A re-examination of modeled and measured soil moisture spatial variability and its implications for land surface modeling. *Adv. Water Resour.* 24:1069-1083.
- Piepmeyer, J.R., and A.J. Gasiewski. 2001. High-resolution passive microwave polarimetric mapping of ocean surface wind vector fields. *IEEE Transaction on Geoscience and Remote Sensing.* 39:606-622.
- Prevot, L., R. Bernard, O. Taconet, D. Vidal-Madjar, and J.L. Thony. 1984. Evaporation from a bare soil evaluated using a soil water transfer model and remotely sensed surface soil moisture data. *Water Resour. Res.* 20:311-316.
- Reichle, R., D. McLaughlin, and D. Entekhabi. 2002. Hydrologic data assimilation with the ensemble Kalman filter. *Mon. Weather Rev.* 130(1):103-114.
- Renschler, C.S. 2003. Designing geo-spatial interfaces to scale process models; the GeoWEPP approach; application of geographic information systems and remote sensing for quantifying patterns of erosion and water quality. *Hydrol. Process.* 17(5):1005-1017.

- Rodriguez-Iturbe, I., M. Marani, R. Rigon, and A. Rinaldo. 1994. A self-organized river basin landscape: Fractal and multifractal characteristics. *Water Resour. Res.* 30(12):3531-3539.
- Rodriguez-Iturbe, I., G.K. Vogel, R. Rigon, D. Entekhabi, F. Castelli, and A. Rinaldo. 1995. On the spatial organization of soil moisture fields. *Geophysics Res. Letters.* 106: 2757-2760.
- Schlosser, A.C., P.C.D. Milly. 2000. The potential impact on the soil moisture initialization on the soil moisture predictability and associated climate predictability. GEWEX/BAHC International Workshop on Soil Moisture Monitoring, Analysis and Prediction for Hydrometeorological and Hydroclimatological Applications. Workshop Summary Report. Norman, OK.
- Schmugge, T.J., P. Gloersen, T. Wilheit, and F. Geiger. 1974. Remote sensing of soil moisture with microwave radiometers. *Soil Sci. Soc. Am. Proc.* 28:721-724.
- Schmugge, T.J., J.M. Meeneely, A. Rango, and R. Neff. 1977. Satellite microwave observations of soil moisture variations. *Water Resour. Bull.* 13:265-286.
- Schmugge, T.J., T.J. Jackson, and H.L. McKim. 1980. Survey of methods for soil moisture determination. *Water Resour. Bull.* 16:961-979.
- Schreier, H., and S. Brown. 2001. Scaling issues in watershed assessments. *Water Policy* 3:475-489.
- Sellers, P.J., M.D. Heiser, F.G. Hall, S.J. Goetz, D.E. Strebel, S.B., Verma, R.L., Desjardins, P.M. Schuepp, and J.I. MacPherson. 1995. Effects of spatial variability in topography, vegetation cover and soil moisture on area-averaged surface fluxes. A case study using FIFE 1989 data. *J. Geophys Res.* 100:25607-25629.
- Simunek, J., M. Sejna, M.T. van Genuchten, J. Majercak, V. Novak, and J. Sutor. 1997. The HYDRUS-ET software package for simulating the one-dimensional movement of water, heat and Multiple solutes in a variably saturated media. Version 1.1. U.S Salinity Lab., USDA-ARS, Riverside, CA, Institute of Hydrology Slovak Academy of Sciences, Bratislava, Slovakia.
- Smith, M.R., and R.W. Newton. 1983. The prediction of root zone soil moisture with a water balance-microwave emission model. AgRISTARS. SM-T3-04425. NASA/GSFC.
- Starks, P.J., G.C. Heathman, L.R. Ahuja, and L. Ma. 2003. Use of limited soil property data and modeling to estimate root zone soil water content. *J. Hydrol.* 272:131-147.

- Starr, J.L., and I.C. Paltineanu. 1998. Soil water dynamics using multisensor capacitance probes in nontraffic interrows of corn. *Soil Sci. Soc. Am. J.* 62:114–122.
- Tessier, Y., S. Lovejoy, and D. Schertzer. 1993. Universal multifractal: Theory and observations for rain and clouds. *Journal of Applied Meteorology.* 32:223-250.
- Thielen, A.H., A. Lücke, B. Diekkrüger and O. Richter. 1999. Scaling input data by GIS for hydrological modeling. *Hydrol. Process.* 13:611-630.
- van Genuchten, M.Th. 1980. A closed-form equation for predicting the hydraulic conductivity of unsaturated soils. *Soil Sci. Am. J.* 44:892-898.
- Vinnikov, K.Y., and A. Robock. 1996. Scales of temporal and spatial variability of midlatitude soil moisture. *J. Geophys. Res.* 101:7163-7174.
- Walker, J.P., G.R. Willgoose, and J.D. Kalma. 2001. One-dimensional soil moisture profile retrieval by assimilation of near-surface observations: A comparison of retrieval algorithms. *Adv. Water Resour.* 24:631–50.
- Western, A.W., and G. Blöschl. 1999. On the spatial scaling of soil moisture. *J. Hydrol.* 217:203-224.
- Western, A.W., R.B. Grayson, G. Blöschl, and D.J. Wilson. 2003. Spatial variability of soil moisture and its implications for scaling. p.119-142. In: Y. Perchepsky, M. Selim and D. Radcliffe (eds.), *Scaling Methods in Soil Physics*. CRC Press, Boca Raton, FL.
- Wickel, A.J., T.J. Jackson, and E.F. Wood. 2001. Southern Great Plains hydrology experiment. *Int. J. Remote Sens.* 22(8):1571–1583.
- Wilson, J.P., and J.C. Gallant. 2000. *Terrain Analysis: Principles and Applications*. John Wiley. Hoboken. NJ.
- Wood, E.F. 1994. Scaling, soil moisture and evapotranspiration into runoff model. *Adv. Water Resour.* 17:25-34.
- Zhu, J., and B.P. Mohanty. 2002. Upscaling of hydraulic properties for steady state evaporation and infiltration. *Water Resour. Res.* 38(9):1178, doi:10.1029/2001.
- Zhu, J., and B.P. Mohanty. 2003a. Effective hydraulic parameters for steady state vertical flow in heterogeneous soils. *Water Resour. Res.* 39(8):1227, doi:10.1029/2002.
- Zhu, J., and B.P. Mohanty. 2003b. Upscaling of hydraulic properties of heterogeneous

soils. p.97-117. In Y. Pachepsky, D.E. Radcliffe, and H. M. Selim, (eds.) *Scaling Methods in Soil Physics*. CRC Press, Boca Raton, FL.

## VITA

Narendra N. Das, son of Basant and Surajmati Das, was born in Bhilai on January 15, 1970. After graduating from S.S. School Sector-10, Bhilai, in 1988, he secured a Bachelor of Engineering degree in chemical engineering at Government Engineering College Raipur in Chattisgarh, India in 1992. He then worked as a manager (I.T.) in Bhilai Steel Plant, Steel Authority of India Limited for a period of ten years. He enrolled in graduate school at Texas A&M University, College Station in the fall 2003 and has been working since then as a graduate research assistant in the Department of Biological & Agricultural Engineering. His permanent address is: Qno-14a, Street-23, Sector-10, Bhilai, Chattisgarh, India.